Quantification of trace element atmospheric deposition fluxes to the Atlantic Ocean (>40°N; GEOVIDE, GEOTRACES GA01) during spring 2014

Rachel U. Shelley, Montserrat Roca-Martí, Maxi Castrillejo, Virginie Sanial, Pere Masqué, William Landing, Pieter van Beek, Hélène Planquette, Géraldine Sarthou

Shelley, R. U., Roca-Martí, M., Castrillejo, M., Sanial, V., Masqué, P., Landing, W. M., van Beek, P., Planquette, H. and Sarthou, G.: Quantification of trace element atmospheric deposition fluxes to the Atlantic Ocean (>40°N; GEOVIDE, GEOTRACES GA01) during spring 2014, Deep Sea Research Part I: Oceanographic Research Papers, 119, 34–49, doi:10.1016/j.dsr.2016.11.010, 2017

Quantification of trace element atmospheric deposition fluxes to the Atlantic Ocean (> 40°N; GEOVIDE, GEOTRACES GA01) during spring 2014☆

Rachel U. Shelley[a,*], Montserrat Roca-Martí[b], Maxi Castrillejo[b], Virginie Sanial[c], Pere Masqué[b,d,e], William M. Landing[f], Pieter van Beek[g], Hélène Planquette[a], Géraldine Sarthou[a]

[a] *Laboratoire des Sciences de l'Environnement Marin, UMR 6539 LEMAR (CNRS/UBO/IRD/IFREMER), Institut Universitaire Européen de la Mer, Technopôle Brest-Iroise, Plouzané 29280, France*
[b] *Departament de Física and Institut de Ciència i Tecnologia Ambientals, Universitat Autònoma de Barcelona, 08193 Bellaterra, Barcelona, Spain*
[c] *School of Natural Sciences, Edith Cowan University, 270 Joondalup Drive, Joondalup, WA 6027, Australia*
[d] *Department of Marine Chemistry and Geochemistry, Woods Hole Oceanographic Institution, Woods Hole, Massachusetts 02543, USA*
[e] *Oceans Institute and School of Physics, The University of Western Australia, 35 Stirling Highway, Crawley, WA 6009, Australia*
[f] *School of Earth, Ocean and Atmospheric Science, Florida State University, 117 N. Woodward Ave., Tallahassee, FL 32306, USA*
[g] *Laboratoire d'Etudes en Géophysique et Océanographie Spatiales (LEGOS), (CNRS-CNES-IRD-UPS), Observatoire Midi Pyrénées, 14 avenue Edouard Belin, Toulouse, 31400, France*

ARTICLE INFO

Keywords:
Atmospheric deposition fluxes
Trace elements
^{7}Be
Atlantic Ocean
GEOTRACES

ABSTRACT

Atmospheric deposition is an important input route of trace elements (TEs) to the global ocean. As atmospheric inputs impact phytoplankton community health and dynamics, atmospheric TE fluxes, and in particular atmospheric iron fluxes, are a key component of marine biogeochemical models. Trace element concentrations were determined in dry (aerosols) and wet (precipitation) deposition samples from the North Atlantic, north of 40°N, during the GEOVIDE cruise (GEOTRACES cruise GA01) in May/June 2014. Atmospheric aerosol loading in the study region was low (~ 2–500 ng m^{-3}) throughout the cruise, as inferred from the very low aerosol Ti concentrations determined (0.0084–1.9 ng m^{-3}). Wet deposition appeared to be of roughly equal or greater importance than dry deposition to the total depositional flux of TEs, which is consistent with other regions of the Atlantic Ocean outside of the influence of the Saharan plume.

It can be challenging to convert aerosol chemical composition data into reliable flux estimates, due to the uncertainties associated with the parameterisation of dry deposition velocity, and precipitation rate.

Therefore, the goal of this study was to compare TE flux estimates derived from two different techniques: (1) the traditional approach of summed wet and dry deposition TE fluxes, using concentration data, precipitation rates, and dry deposition velocities and, (2) using the inventory of the cosmogenic radioisotope beryllium-7 (^{7}Be) in the upper ocean as a proxy for atmospheric deposition. These two approaches yielded TE flux estimates that were in excellent agreement (within one standard deviation) for about half of the TEs under investigation. However, for the remaining TEs differences between the flux estimates ranged from two to forty times, with the traditional approach generally being the higher of the two estimates. Therefore, factors that may contribute to this variation, such as differences in the timescale of integration and selection of representative deposition velocities and precipitation rates, are discussed. Our results suggest that the ^{7}Be approach continues to show promise in this application, particularly in regions where precipitation samples cannot be routinely collected.

1. Introduction

Atmospheric deposition is an important input route of trace elements (TEs) to the global ocean, and can be the principal input in some open ocean regions (Jickells et al., 2005). Atmospheric deposition is delivered to the surface ocean via wet (rain, fog, snow) and dry deposition (dust, soil, ash). It is important to quantify the total atmospheric deposition fluxes of TEs (both essential and potentially deleterious) to the surface ocean as atmospheric inputs impact phytoplankton community health and dynamics. Thus, in this way,

☆ All authors have approved the final article.

* Corresponding author.
E-mail address: rachel.shelley@univ-brest.fr (R.U. Shelley).

atmospheric TE inputs may be linked to the global C and N cycles, key players in the global climate system (Morel and Price, 2003; Sunda, 2012). Yet many areas of the global ocean are limited, or co-limited by TE availability (Saito et al., 2008; Moore et al., 2013). Understanding the processes that govern TE supply and availability are key for gaining a mechanistic understanding of the biological carbon pump. However, atmospheric deposition remains poorly constrained, largely due to the difficulties associated with quantifying fluxes (Law et al., 2013).

The magnitude of aerosol input to the atmosphere from dust producing regions is a function of wind speed and precipitation in those regions. The magnitude of aerosol deposition downwind from aerosol source regions is a function of atmospheric loading, particle size and type, wind speed, humidity and precipitation in the receiving areas (Moulin et al., 1997). Even in the North Atlantic Ocean, which receives the largest inputs due to its proximity to the Sahara Desert (~40% of annual global dust deposition; Jickells et al., 2005), aerosol deposition is not uniformly distributed. The Sahara outflow transports vast quantities of mineral dust (~1×10^{12} t a year; d'Almeida, 1986) over the Atlantic Ocean, as far as the Americas, at altitudes above the marine boundary layer (MBL; ~500–6000 m; Prospero and Carlson, 1972), approximately over the latitudinal band 5–30°N. To the south, the Saharan dust plume is largely constrained by the seasonally-migrating intertropical convergence zone (ITCZ; ~5–10°N) (Prospero and Carlson, 1972; Doherty et al., 2012; Schlosser et al., 2013), and to the north by the northern extent of the trade winds (~30°N). North of 30°N, a steep declining gradient in atmospheric aerosol loading, as determined by metrics such as aerosol optical depth (AOD; e.g. http://aeronet.gsfc.nasa.gov), is observed due to a combination of increasing distance from North African dust source regions and large-scale atmospheric circulation. As a result, other aerosol sources (Europe, North America, sea salt and, occasionally, volcanoes) become relatively more important in the north of this ocean basin. Thus, several aerosol sources are likely to contribute to the TE composition of the bulk aerosol.

The objectives of this study were to (1) investigate aerosol sources of a suite of TEs of interest to the GEOTRACES programme (www.geotraces.org); and (2) quantify the atmospheric deposition flux of TEs to surface waters of the North Atlantic at latitudes greater than 40°N. In order to do this, TE fluxes were calculated using, 1) the traditional approach of deriving fluxes from the summation of TE concentration data from wet and dry deposition (e.g., Duce at al., 1991), and 2) a novel tracer approach which uses the natural cosmogenic radionuclide Beryllium-7 (^{7}Be) as a tracer for atmospheric inputs (Cámara-Mor et al., 2011; Kadko and Prospero, 2011; Kadko et al., 2015, 2016). The two approaches resulted in flux estimates that were in excellent agreement for approximately half the TEs under investigation, but performed less well for the remaining TEs, with differences of 2–40 times between them. Therefore, potential sources of uncertainties are discussed.

2. Methods

The *GEOVIDE* campaign (*GEOTRACES* cruise *GA01*; 15 May-30 June 2014), on board the *N/O Pourquoi Pas?*, departed from Lisbon, Portugal, and sailed northwest following the *OVIDE* line (http://wwz.ifremer.fr/lpo/La-recherche/Projets-en-cours/OVIDE) to the Greenland shelf, after which the ship entered the Labrador Sea and sailed for the final port of St John's, Newfoundland, Canada (Fig. 1). In total, 18 aerosol samples and 10 precipitation samples were collected for the determination of a suite of TEs. In addition, ^{7}Be was determined from 18 aerosol samples, 8 precipitation samples, and 9 relatively shallow water column profiles.

2.1. Sample collection and analysis

Aerosol TEs: Samples were collected using a mass flow-controlled,

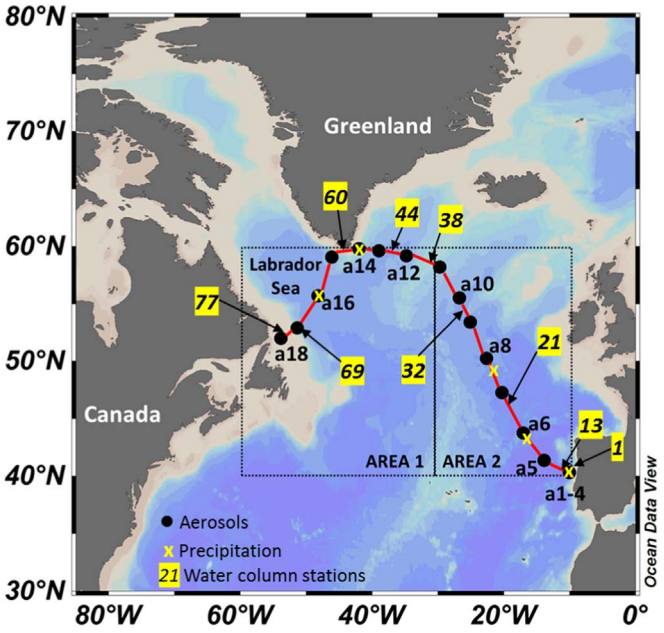

Fig. 1. The *GEOVIDE* cruise track. Aerosol samples *geoa*1–4 (displayed as "a1-4") were collected in close proximity, thus are only shown as one dot on the above map. There were ten precipitation events; the first six ocurred at the same location as aerosol samples *geoa*1–4. The dashed lines indicate the boxes, Area 1 and Area 2; the dividing line is located at 30°W (further details can be found in the Methods). Water column sampling stations are indicated by the arrows; the station numbers are highlighted in yellow. Metadata for the aerosol, rain and water column sample locations can be found in Tables S1, S2 and S3, respectively (Supplemental Material).

high volume aerosol sampler (~1 m^{-3} min^{-1}; model TE 5171, Tisch Environmental). The aerosol sampler was sector (± 60° from the bow) and wind speed (< 0.9 m s^{-1}) controlled, to minimise the risk of contamination from the ship's exhaust stack, using an anemometer and vane attached to a 3 m pole mounted on the railings near the aerosol sampler. The aerosol sampler was positioned on the forward railings (starboard side) on the flight deck above the bridge (~15 m above sea level). Twelve replicate samples were collected on acid-washed, 47 mm diameter Whatman 41 (W41) ashless filter discs (mixed cellulose esters; total exposed area 149 cm^{2}), which were positioned on a 12-position PVC adapter plate (Shelley et al., 2015). The first sample collected represented a 24 h deployment (sample time =19.6 h), but after visual inspection of the filters and of air mass back trajectory simulations (using the Hybrid Single Particle Lagrangian Integrated Trajectory Model, HYSPLIT), it became apparent that this sampling duration would be insufficient to collect enough material on the filters. Thus, the deployment time was increased to 48 h (sample time =17.4 – 47.6 h) for all subsequent samples. After recovery, filters were removed from the filter holders inside a laminar flow bench, placed in individual petri-slides (Merck), double ziplock bagged, and immediately frozen (−20 °C) for storage. Three of the twelve replicate samples were reserved for determination of ^{7}Be.

On return to the home laboratory, the aerosol samples were digested to determine concentrations of a suite of TEs by high resolution, magnetic sector field inductively coupled plasma mass spectrometry (SF-ICP-MS; Element 2, Thermo-Fisher). The TEs determined were: Al, P, Ti, V, Cr, Mn, Fe, Co, Ni, Cu, Zn, Sr, Y, Zr, Mo, Ag, Cd, Ba and Pb. This list includes lithogenic tracers (Al, Ti, Y, Zr), a suite of bioactive elements (P, V, Cr, Mn, Fe, Co, Ni, Cu, Zn, Mo, Cd), and pollution-derived TEs with no known biological role (Ag and Pb). All filter digestions were performed under Class-100 laminar flow conditions following the protocol of Morton et al. (2013). Briefly, the W41 filter discs were digested in tightly-capped 15 mL Teflon-PFA vials (Savillex) using sequential additions of (1) 500 µL of nitric acid (HNO_3; 15.8 M, Ultrapur, Merck); and (2) 1 mL of HNO_3 (15.8 M, Ultrapur,

Merck) plus 200 μL of hydrofluoric acid (HF; 32 M, Ultrapur, Merck). During both steps the solutions were heated to 150 °C, and were taken to near-dryness after each step. After the final digestion and evaporation, the samples were re-dissolved in 15 mL of 0.4 M HNO_3 (Ultrapur, Merck) containing 1 ppb indium (In) as an internal standard for drift correction. For analysis by SF-ICP-MS, 2 mL of this solution was further diluted in acid-washed, rounded bottom, polypropylene centrifuge tubes (VWR) by addition of 2 mL of the same batch of 0.4 M HNO_3 containing 1 ppb In. Samples were introduced to a PFA-ST nebulizer (Elemental Scientific Incorporated) via a modified SC-Fast introduction system consisting of an SC-2 autosampler, a six-port valve and a vacuum rinsing pump. Blank solutions for the acid digestions were prepared by digesting W41 discs that had been deployed in the aerosol sampler for 1 h while the pumps were not in operation, and the resulting concentrations were subtracted from all acid-digested filter samples. Blank values can be found in Table S1 (Supplemental Material).

In order to assess the homogeneity of the twelve replicate sample filters every fourth sample was analysed in triplicate. For Fe, for example, this resulted in precision (relative standard deviation between replicate samples) that was less than 10% for all but the lightest-loaded sample (0.68 ± 0.19 ng m^{-3}), which was close to the detection limit. In order to investigate digestion efficiency and recovery, two separate reference materials were digested. The reference materials digested were: National Research Council of Canada lake sediment (LKSD-1; composition data compiled in the GeoReM database; http://georem.mpch-mainz.gwdg.de/); and Arizona Test Dust (ATD; nominal 0–3 μm, Powder Technology Inc.). The Landing Laboratory at Florida State University is currently investigating the use of ATD as a dust reference material, and is compiling a database of elemental abundances. The ATD will become more suitable for distribution as a dust reference material as other laboratories contribute concentrations to the consensus reference material effort (sub-samples are available on request from: wlanding@fsu.edu). Further discussion of the use of ATD as a reference material, and elemental abundance data is presented in Table 1 of Shelley et al. (2015). Values for LKSD-1 and ATD from this study are presented in Table S1.

Precipitation TEs: Rain samples were collected on an event basis using a Teflon precipitation sampler that was fabricated in-house at the Laboratoire des sciences de l'Environnement MARin (LEMAR; Cheize et al., 2012). An acid-cleaned 1 L HDPE bottle was attached to the sampler by means of a Teflon screw fitting. The cover of the rain sampler was removed manually on commencement of a rain event, and replaced after the rain had stopped. The sample was immediately removed from the sampler and the sample bottle replaced with a new, clean 1 L bottle. Samples were acidified to 0.024 M HCl (Ultrapur, Merck) inside a laminar flow bench at sea, and double bagged for storage. On return to the home laboratory, the samples were shaken vigorously, and ~2 mL of sample was pipetted in to Teflon beakers. The aliquot was evaporated on a hotplate positioned inside a laminar flow bench. The resulting residue was re-dissolved in 4 mL 0.4 M HNO_3 (Ultrapur, Merck) prior to determination by SF-ICP-MS of the same suite of TEs as the aerosol samples (except strontium (Sr) and silver (Ag) which were not determined in the precipitation samples). Precipitation sample volumes ranged from 13 to 1120 mL. The TE concentration data and metadata for the precipitation samples can be found in Table S2 (Supplemental material).

Determination of ^{7}Be in seawater, bulk deposition (precipitation) and aerosol samples: Seawater samples (n=28, 50–100 L each) were collected from three to four depths spanning from the surface (5 m) to about 100 m below the mixed layer (Fig. S2, Supplemental material), using a stainless steel CTD rosette and standard Niskin bottles equipped with rubber feathers instead of steel springs. Bulk deposition samples (n=8, 0.16–2.6 L each) were collected over one to eight day intervals, depending on the sample volume and the proximity to water column stations, using a homemade bulk deposition sampler (1.5 m high, 25 cm diameter) similar to the one used for TE precipitation collection. The ^{7}Be bulk deposition sampler was positioned close to the TE precipitation sampler to ensure similar sampling conditions. However, in contrast to the TE precipitation collections, which were on an event basis to minimise the risk of contamination, the ^{7}Be bulk deposition samplers remained open and uncovered at all times. Seawater and precipitation samples were treated following the protocols of Cámara-Mor et al. (2011). Briefly, samples were acidified with 37% HCl (Panreac/QP) to pH ~1 and spiked with 5 mg of stable Be as a yield tracer. After addition of Fe^{3+} as a carrier and vigorous stirring, samples were allowed to equilibrate for 12 h. Beryllium was then co-precipitated with iron hydroxides by adjusting the pH to ~8.5 using 30% NH_3 (Panreac/QP). The supernatant was carefully removed via siphoning and the precipitate was transferred to 250 mL plastic bottles and stored until further analysis at the Universitat Autònoma de Barcelona (UAB). Aerosol samples (n=18) were collected as described above for TEs and stored frozen until determination of ^{7}Be. At the UAB, Fe precipitates from seawater and precipitation samples were dissolved in 2 M HCl (Panreac/QP) and transferred to hermetically sealed PE vials for gamma counting. ^{7}Be gamma emissions (477.6 keV) were measured within three months of sample collection using well-type, high-purity Ge detectors located either at the Universitat Autònoma de Barcelona or at the LAFARA underground laboratory in the French Pyrénées (van Beek et al., 2013). The low background at the LAFARA underground laboratory allowed us to detect low ^{7}Be activities in the samples, which was especially the case for the deepest seawater samples. Detectors were calibrated for the correct vial geometry by measuring a commercial standard solution (MCR-2009-018) of known gamma activities (60–1836 keV) or IAEA-RGU1, IAEA-RGTH1 and IRSN-135SL300 standard materials. For aerosol samples, the three filters were processed together. Each set of three filters was spiked with 2 mg of stable Be as a yield tracer, digested using a mixture of concentrated HNO_3, HCl and HF at a ratio of 10:4:6 (Panreac/technical and analytical grade), re-dissolved with 2 M HCl, placed in vials and measured by gamma spectrometry as described for the seawater and precipitation samples. After counting, one aliquot from each sample was taken to determine the chemical recovery of stable Be by inductively coupled plasma optical emission spectrometry (ICP-OES), which averaged 88%. ^{7}Be activities were corrected for decay to collection date. The ^{7}Be data and metadata for aerosol, precipitation and seawater samples can be found in Table S3 (Supplemental Material).

Table 1
Bulk deposition velocities ($P_R \times_R \times \rho + V_d$) for mineral dust (e.g. Al) and ^{7}Be over the precipitation rate range 0.5–7 mm d^{-1}.

Al		^{7}Be	
S_R	200[a,b]	640[c]	
V_d (m d^{-1})	1000[a]	294[c]	
P_R	Bulk V_d	Bulk V_d	Al/ ^{7}Be bulk V_d
mm d^{-1}	m d^{-1}	m d^{-1}	ratio
0.5	1083	560	1.9
1	1167	827	1.4
2	1333	1360	1.0
3	1500	1893	0.8
4	1667	2427	0.7
5	1833	2961	0.6
6	2000	3494	0.6
7	2167	4027	0.5

[a] Duce et al. (1991).
[b] Jickells and Spokes (2001).
[c] Akata et al. (2008).

2.2. Air mass back trajectories

Five-day (120 h) air mass back trajectories were simulated for each

aerosol sampling interval (Fig. S1, Supplemental Material) using the GDAS meteorology in the publicly available NOAA Air Resources Laboratory Hybrid Single-Particle Lagrangian Integrated Trajectory (HYSPLIT) model (Stein et al., 2015; Rolph, 2016). The normal form of the model was used, with arrival heights of 50, 500 and 1500 m, in order to investigate the behaviour and fate of aerosols in and above the MBL, typically 400–1200 m thick). With the exception of samples *geoa*9, *geoa*16-18 (European and Canadian origins, respectively), all air mass back trajectories during this study were defined as Remote Marine, meaning that the air masses had had little to no interaction with major continental land masses within the simulation period.

2.3. Positive matrix factorisation (PMF)

Multivariate statistical analysis methods provide a powerful tool for looking at patterns in large data sets and/or datasets that include many parameters. Receptor models use multivariate statistical techniques that can be used to identify and quantitatively apportion pollutants to their sources by looking for trends, and identifying potential markers for the sources (Comero et al., 2009). The United States Environmental Protection Agency (EPA) has developed a receptor model for analysis of environmental quality data that is freely available online (available at: http://www.epa.gov/air-research/positive-matrix-factorisation-model-environmental-data-analyses). Positive Matrix Factorisation (PMF) reduces the dimensions of complex data sets to a smaller number of factors, which are used to identify potential sources.

Although the US EPA environmental quality monitoring sites are at fixed locations (as opposed to multiple sites along an oceanographic transect), PMF may still be able to provide insights into potential aerosol sources, especially when used in conjunction with air mass back trajectory simulations and enrichment factors. The EPA PMF model (v. 5.0) was used in this study to look for trends in the *GEOVIDE* aerosol TE data set. A detailed description of how to interpret the model outputs and error estimation results can be found in the EPA PMF user guide (http://www2.epa.gov/sites/production/files/2015-02/documents/pmf_5.0_user_guide.pdf). Briefly, "Base Model Runs" produce the primary output of profiles and factor contributions. The base model run uses a random seed (starting point) for iterations, and generates a value for goodness of fit; the Q-value. The iteration with the lowest Q-(robust) value is highlighted in the output, and the analysis based on this iteration should be used to interpret the model output.

Although the EPA-PMF model cannot conclusively define the sources represented by the factors, it does allow the user to identify markers for the sources based on *a priori* knowledge of potential aerosol sources (e.g., lithogenic TEs such as Al and Ti for mineral dust, or V and Ni for shipping emissions). The application of the EPA-PMF model in this study was exploratory, in the sense that all data was included without any attempt to weight individual data points identified as outliers. However, sample *geoa*16 and 18 were excluded from the PMF analysis, due to concentrations below the detection limit for Cr, Y and Zr (*geoa*16), and Ni and Zn (*geoa*18), as the model is unable to process blank cells, and it is inappropriate to interpolate aerosol TE data. Samples were removed rather than TEs to maximise the number of TEs that could serve as markers for source apportionment. A two, three and four factor model was fitted to the aerosol TE data. However, due to the small number of samples only the two factor model was well-constrained in terms of error estimation. The two factors were identified as: (1) mineral dust (highest contributions from Zr and Y), and (2) a factor that was dominated by Sr, but also had high contributions from Cu, V and Ni.

2.4. Atmospheric deposition flux estimations

The atmospheric deposition of trace elements to the ocean is a key parameter in biogeochemical models, yet it remains poorly constrained, largely as a result of the difficulty in collecting representative samples from remote oceanographic settings, and the challenge of converting aerosol chemical concentration data into realistic flux estimates. In the Atlantic Ocean, chemical composition data has been collected from both island-based sites, e.g., from long-term atmospheric observatories, such as the AEROCE sites in the North Atlantic Ocean (Bermuda, Barbados, Mace Head, Izaña; e.g. Prospero et al., 2014; Sholkovitz et al., 2009), and from large-scale oceanographic campaigns, such as the Atlantic Meridional Transect (Baker et al., 2006, 2013), *CLIVAR* Repeat Hydrography cruises (Buck et al., 2010) and *GEOTRACES* cruises (Shelley et al., 2015), as well as from numerous regional-scale oceanographic campaigns (e.g. Stuut et al., 2005).

As atmospheric deposition is both spatially and temporally variable, in order to minimise the effect of outliers in the aerosol chemical concentration data we have chosen to take a box approach to estimate atmospheric deposition fluxes over our study area in late spring/early summer 2014. We base our atmospheric deposition boxes on the areas defined in Baker et al. (2010), which they based on the distribution of rainfall over the Atlantic Ocean (Xie and Arkin, 1997). However, as this study occupied stations further north than Baker et al. (2010), we have extended the boxed regions by approximately 10° in a northerly direction to include the most northerly section of our study area. Therefore, the regions we define are Area 1 (western section of transect, > 30°W) and Area 2 (eastern section of transect, < 30°W) (Fig. 1).

2.5. Dry deposition flux estimation

Dry deposition fluxes of TEs, F_{dry}, were calculated using the following equation:

$$F_{dry} = C_{atmos} \times V_d \quad (1)$$

Where C_{atmos} is the concentration of the species of interest in the aerosol, and V_d is the dry deposition velocity. The largest source of error (up to a factor of 3) in this calculation is associated with the choice of V_d (Duce et al., 1991). Deposition velocity is sensitive to fluctuations in wind speed, relative humidity and particle size (Slinn and Slinn, 1981), and while wind speed and particle size dependent parameterisations are available (e.g. Ganzeveld et al., 1998), these, too, are subject to uncertainties. As a result, fixed V_d values are still commonly used.

2.6. Wet deposition flux estimation

Wet deposition TE fluxes, F_{wet}, were calculated using the following equation:

$$F_{wet} = C_{rain} \times P_R \quad (2)$$

Where C_{rain} is the concentration of the element of interest in rain water and P_R is the precipitation rate. However, accurate representation of precipitation rates can be problematic in remote ocean regions. Rain collector efficiency is very sensitive to wind speed, thus, in order to obtain accurate rainfall rates wind screens are required (Sieck et al., 2007). This presents a significant obstacle to determining accurate precipitation rates from samples collected at sea, where samplers are located on exposed platforms high on the ship, and sampling occurs while the ship is facing into the oncoming wind and/or while underway, as wind screens are not routinely deployed on rain samplers at sea. Furthermore, rain samples are usually only collected from events that occur along the planned cruise track, consequently nearby events are missed, as are ones that occurred prior to station occupation. Other sources of wet deposition, such as fog and snow can be difficult to collect, and their deposition rates may be even more difficult to quantify than rain rates. Thus, researchers may rely on climatologies from satellite products, which, themselves, may be subject to large uncertainties. With this in mind, the precipitation data used in this

study was obtained from the NASA Giovanni satellite data product (http://giovanni.sci.gsfc.nasa.gov/giovanni/) using TRMM and GPM sources. A time-averaged (May–June 2014) map of multi-satellite precipitation estimates, with 0.1° resolution was used in combination with a plot of area-averaged precipitation rate estimates for the eastern section of the study area (Figs. S2a and S2b, Supplemental Material), resulting in precipitation rate estimates from 0 to 3.6 mm d^{-1} along the cruise track (Fig. S3a). For the wet deposition flux estimates we chose a value close to the mid-point of this range, 2.0 mm d^{-1}. This value was also chosen as it reflects the low end of the range of precipitation rates determined from the ^{7}Be precipitation collections (2.2–6.7 mm d^{-1}). This value corresponds to the low end of the range of precipitation rates determined from the ^{7}Be precipitation collections.

An additional source of error in wet deposition flux estimations may result from the sensitivity of species concentration on sample volume, due to a dilution effect (Jaffrezo et al., 1990). Therefore, to mitigate any volume effects, we calculated a volume weighted mean (VWM) rain concentration (C_{rain}) for each of the two boxed areas used in this study, from the product of the rainfall concentrations (C_i) and volumes (V_i) (Eq. (3)).

$$C_{rain} = \sum C_i V_i \; / \; \sum V_i \quad (3)$$

2.7. Total deposition flux estimation (^{7}Be approach)

An alternative to the traditional approach for the estimation of the total deposition fluxes of TEs (summed wet and dry deposition fluxes) described above is the use of ^{7}Be as a proxy for atmospheric deposition as described by Kadko et al. (2015, 2016). This cosmogenically-formed radioisotope ($T_{1/2}$ of 53.3 days) is deposited to the ocean predominantly via precipitation, and is subsequently homogenised in the mixed layer (Silker, 1972; Kadko and Olson, 1996). As the water column inventory represents an integration of the input over approximately the previous 2.5 months (the mean life-time of ^{7}Be is 77 days), ^{7}Be can be used as a tracer of atmospheric deposition on seasonal timescales. This approach assumes that the only loss term for ^{7}Be from the water column is radioactive decay.

The total deposition fluxes of the species of interest are derived from the following equation, using ^{7}Be as an example:

$$F_{total,\ Be7} = C_{Be7} \times (P_R \times S_R \times \rho + V_d) \quad (4)$$

Where the total deposition flux of ^{7}Be (dpm m^{-2} d^{-1}), $F_{total,\ Be7}$, is derived from the ^{7}Be inventory in the upper water column (dpm m^{-2}, ocean ΣBe7) multiplied by the ^{7}Be radioactive decay constant (λ=0.013 d^{-1}), and C_{Be7} is the concentration of ^{7}Be in the bulk aerosol (dpm m^{-3}). The inventory of ^{7}Be in the mixed layer was calculated considering a homogeneous concentration of ^{7}Be and a mixed layer depth set by the threshold method (taking a threshold value difference of 0.05 kg m^{-3} for the potential density anomaly referenced to the sea surface, Monterey and Levitus, 1997; Thomson and Fine, 2003). Below the mixed layer, the inventory of ^{7}Be was calculated assuming an exponential decrease from the base of the mixed layer to the depth where the ^{7}Be concentration was 1% of that in the mixed layer. P_R is the precipitation rate (m d^{-1}), S_R is the scavenging ratio, and ρ is the density of liquid water divided by the density of air (~1000 kg m^{-3}/ 1.2 kg m^{-3}=~833). The first three terms in the brackets of Equation 4, P_R, S_R and ρ, describe the wet deposition velocity, whereas V_d is the dry deposition velocity (m d^{-1}); when summed these terms describe the bulk deposition velocity. As the open ocean is generally a low particle regime, $T_{1/2}$ of ^{7}Be is short and atmospheric inputs are relatively large, losses via particle scavenging in the water column are assumed to be negligible. Thus, Equation 5 is an alternative way of writing Equation 4.

$$F_{total,\ Be7} = ([Ocean\Sigma Be7]\lambda) = C_{Be7} \times Bulk V_d \quad (5)$$

Similarly, we can calculate the flux of atmospheric TEs ($F_{total,\ TE}$) from the bulk V_d (P_R x S_R x ρ+ V_d) and the concentration of TE (C_{TE}) in aerosol (Eq. (6)).

$$F_{total,\ TE} = C_{TE} \times Bulk V_d \quad (6)$$

Assuming that the bulk V_d is the same for both TEs and ^{7}Be, we can then estimate the flux of any aerosol TE from the ocean inventory of ^{7}Be and the TE/^{7}Be ratio in aerosols (Eq. (7)).

$$F_{total,\ TE} = ([Ocean\Sigma Be7]\lambda) \times \frac{C_{TE}}{C_{Be7}} \quad (7)$$

Is it reasonable to assume the bulk V_d is the same for TEs and ^{7}Be? Table 1 shows that while the S_R for mineral dust (represented by Al in Table 1) is relatively small, V_d is relatively large, whereas for ^{7}Be, the opposite is true, thus differences tend to cancel. Jickells and Spokes (2001) estimated a mean S_R for Fe of 200, and Duce et al. (1991) found that the global mean for both Al (lithogenic) and Pb (pollution-derived) was also 200, and, thus, assumed that this value would hold for other TEs in the Atlantic. In contrast, Akata et al. (2008) found that the mean S_R for ^{7}Be was 640, and the V_d ranged from 147 to 10368 m d^{-1} (0.17–12 cm s^{-1}). In Table 1, we have used a V_d of 294 m d^{-1} (0.34 cm s^{-1}) as ^{7}Be is primarily associated with fine mode particles, with a mean size range of 0.5–0.6 μm (Winkler et al., 1998). Thus, Equation 4 allows us to estimate the differences in the bulk V_d term between coarse and fine mode aerosols (Table 1). The bulk V_d for Al was roughly equal to that of ^{7}Be for precipitation rates of ~1–3 mm d^{-1}, which cover the range of precipitation rates estimated for the study area in May/June 2014 from the Giovanni satellite products (Fig. S2, Supplemental Material), but is less than that of ^{7}Be for the precipitation rates estimated from the ^{7}Be precipitation collections (2.2–6.7 mm d^{-1}). This reflects the higher scavenging ratio of ^{7}Be relative to that of Al.

The total deposition flux of ^{7}Be was also estimated from precipitation samples (Table 2c), $F_{total\ (precipitation),\ Be7}$, by using the ^{7}Be activity decay-corrected to mid sampling (A_{Be7}), the time period of collection (t) and the collector surface (S) as shown in Equation 8. The precipitation samples are representative of short periods of time (from 1 to 8 days), while the inventories measured in the water column integrate over the mean life-time of ^{7}Be.

$$F_{total\ (precipitation),\ Be7} = \frac{A_{Be7} \times \lambda}{(1-e^{-\lambda t}) \times S} \quad (8)$$

3. Results and discussion

3.1. Aerosol TE distributions

The lithogenic TEs, Al, Mn, Fe, Ti, Y and Zr, all had similar spatial distributions (Fig. 2; Table S1, Supplemental Material), suggesting common source(s) and atmospheric processing during transport. Both Al and Ti can be used as proxies for mineral dust inputs as it is assumed that they are mostly associated with mineral phases. Given that the abundance of Al and Ti in mean upper crustal (UC) material (a proxy for a mineral dust end member) is known, 8.2 ± 3% and 0.38 ± 0.05%, respectively (Rudnick and Gao, 2003), the abundance of either Al or Ti can be used to estimate total dust concentrations. Throughout the *GEOVIDE* campaign aerosol Ti loading was low (0.0084–1.9 ng Ti m^{-3} air filtered; Fig. 2), and, thus by implication, so too was dust loading. Using the Ti data, this results in estimates of ~2–500 ng of material per m^{-3} air filtered. The region of lowest aerosol Ti and dust loading was in the Southwest Irminger Sea and the Labrador Sea (*geoa*12–16, Ti =0.0084–0.14 ng m^{-3}). As the ship passed on to the Newfoundland shelf aerosol Ti loading, and therefore, atmospheric dust loading increased.

Nickel, Cu, Sr, Mo, Ag and Pb had no clear spatial patterns, suggestive of either one discrete source with variable inputs (e.g., sea salt), or multiple sources (e.g., different industrial sources) along the transect and, with the exception of Sr, likely of primarily anthropogenic

Table 2
Concentrations, inventories and deposition flux estimates of ^{7}Be from (a) aerosols, (b) seawater, and (c) bulk deposition (precipitation) samples (± ^{7}Be counting uncertainty). Note that there is no aerosol ^{7}Be data (Table 2a) from 10 to 23 June 2014 (*geoa*11–16) as ^{7}Be activity was below detection (minimum detectable activity range: 0.019 dpm m^{-3} (*geoa*15) – 0.046 dpm m^{-3} (*geoa*11)) in the Irminger and Labrador Seas. The contribution of dry deposition to total ^{7}Be flux is calculated using the ^{7}Be fluxes derived from aerosol concentrations (Eq. (1)) and those derived from the water column inventories (Eq. (5)) from the same approximate location (station indicated in brackets). An extended version of this table can be found in the Supplemental Material (Table S3).

(a) Aerosols

Area	Sample	Sample date (start)	^{7}Be concentration dpm m^{-3}	Dry ^{7}Be flux dpm m^{-2} d^{-1}	% Contribution of dry deposition to total ^{7}Be flux
2	*geoa*1	19-May-14	0.078 ± 0.017	20 ± 5	13 (1)
2	*geoa*2	23-May-14	0.193 ± 0.019	51 ± 5	
2	*geoa*3	24-May-14	0.35 ± 0.02	92 ± 6	65 (13)
2	*geoa*4	25-May-14	0.230 ± 0.012	60 ± 3	42 (13)
2	*geoa*5	27-May-14	0.17 ± 0.03	44 ± 6	
2	*geoa*6	30-May-14	0.088 ± 0.014	23 ± 4	10 (21)
2	*geoa*7	02-Jun-14	0.114 ± 0.011	30 ± 3	
2	*geoa*8	04-Jun-14	0.112 ± 0.012	29 ± 3	
2	*geoa*9	06-Jun-14	0.109 ± 0.018	28 ± 5	9 (32)
2	*geoa*10	08-Jun-14	0.052 ± 0.009	13 ± 2	
1	*geoa*17	23-Jun-14	0.095 ± 0.011	25 ± 3	19 (69)
1	*geoa*18	25-Jun-14	0.062 ± 0.009	16.0 ± 0.8	12 (77)

(b) Seawater

Area	Station	Sample date	^{7}Be inventory dpm m^{-2}	Total ^{7}Be flux dpm m^{-2} d^{-1}
2	1	20-May-14	11600 ± 400	151 ± 5
2	13	25-May-14	10900 ± 1100	141 ± 14
2	21	01-Jun-14	17100 ± 600	220 ± 8
2	32	08-Jun-14	23300 ± 800	302 ± 10
2	38	11-Jun-14	10600 ± 900	140 ± 12
1	44	14-Jun-14	5700 ± 1000	74 ± 13
1	60	18-Jun-14	11000 ± 300	143 ± 4
1	69	23-Jun-14	9700 ± 300	126 ± 4
1	77	26-Jun-14	10500 ± 300	136 ± 4

(c) Precipitation

Area	Sample	Sample date (start)	^{7}Be concentration dpm m^{-3}	Total ^{7}Be flux dpm m^{-2} d^{-1}
2	*BeR*-1	17-May-14	87000 ± 3000	484 ± 19
2	*BeR*-2	20-May-14	286000 ± 15000	650 ± 30
2	*BeR*-3	28-May-14	99000 ± 3000	334 ± 11
2	*BeR*-4	05-Jun-14	183000 ± 4000	880 ± 20
1	*BeR*-5	10-Jun-14	64600 ± 1800	354 ± 10
1	*BeR*-6	15-Jun-14	49000 ± 1900	349 ± 13
1	*BeR*-7	23-Jun-14	105000 ± 5000	400 ± 20
1	*BeR*-8	26-Jun-14	111000 ± 8000	255 ± 18

origin. The lack of a spatial pattern for Sr deposition could point to a marine source of Sr (Vitousek et al., 1999). However, there was no relationship between the average wind speed and aerosol Sr (r^2 =0.20, p=0.074; Fig. S4, Supplemental Material), suggesting that the Sr during GEOVIDE was not predominantly a cyclic salt (Nair et al., 2005).

The influence of different source regions on aerosol TE composition can result in large differences in TE concentrations in aerosol samples collected in similar areas. For example, the aerosol Al and Fe concentrations in samples collected at 40.3°N, 10.0°W (*geoa*1) and 40.3°N, 12.2°W (*geoa*2) during this study were 9.0 and 21 ng m^{-3} (Al), and 5.1 and 13 ng m^{-3} (Fe), respectively, and five days prior to sampling the air mass had originated over southern Greenland. In contrast, during the *GEOTRACES GA*03 campaign (leg 1, Oct-Nov 2010, Lisbon, Portugal to Mindelo, Cape Verde Islands) an aerosol sample was collected from a nearby location (38.3°N, 9.7°W), which had 1–2 orders of magnitude higher Al and Fe (155 and 147 ng m^{-3}, respectively). An air mass back trajectory simulation of that sample indicated that the sampled aerosol had been transported in an air mass that had previously traversed much of northern and western Europe (Shelley et al., 2015).

As atmospheric aerosol loading was low, compared to regions to the south of our study area (i.e., under the influence of the Saharan dust plume, e.g., Shelley et al., 2015), all but one of the samples (*geoa*9) had no visible material on the filters. Grey material was observed on the filters of sample *geoa*9, which had a western European origin within five days of sample collection (Fig. S1, Supplemental Material). This sample had higher concentrations (i.e., > 1 SD higher) for about half of the TEs (Al, V, Co, Ni, Cu, Zn, Sr, Mo, Cd, Pb), with respect to the previous and following samples (Fig. 2). Most of these TEs (V, Ni, Cu, Zn, Mo, Cd, Pb) are linked with anthropogenic sources, which suggests that aerosol Al, Co and Sr could also have had an anthropogenic component in this sample.

3.2. Aerosol elemental ratios and enrichment factors

Although Al and Ti are equally suited as tracers of mineral dust inputs, it was decided to use Ti in this study, as Ti is less prone to contamination from metal components on the ship. The very low Ti loading (0.0084 ng m^{-3}) of sample *geoa*16 (close to the detection limit) could explain the anomalously high TE/Ti ratios for some elements (Al, P, Zn, Sr, Ba, Pb). For example, the EF of Sr was 127 compared to an average of 3.0 ± 3.3 for the remaining samples (Table S4). This was less of a problem for the data normalised to Al, but it should be noted that for Sr, Ba and Pb the elemental ratios were still anomalously high for *geoa*16 whether the data was normalised to Al or Ti. Alternatively, sample *geoa*16 may have been contaminated for the TEs with anomalously high elemental ratios. Whatever the reason, these anomalously high elemental ratios resulted in the decision to exclude this sample from the following discussion.

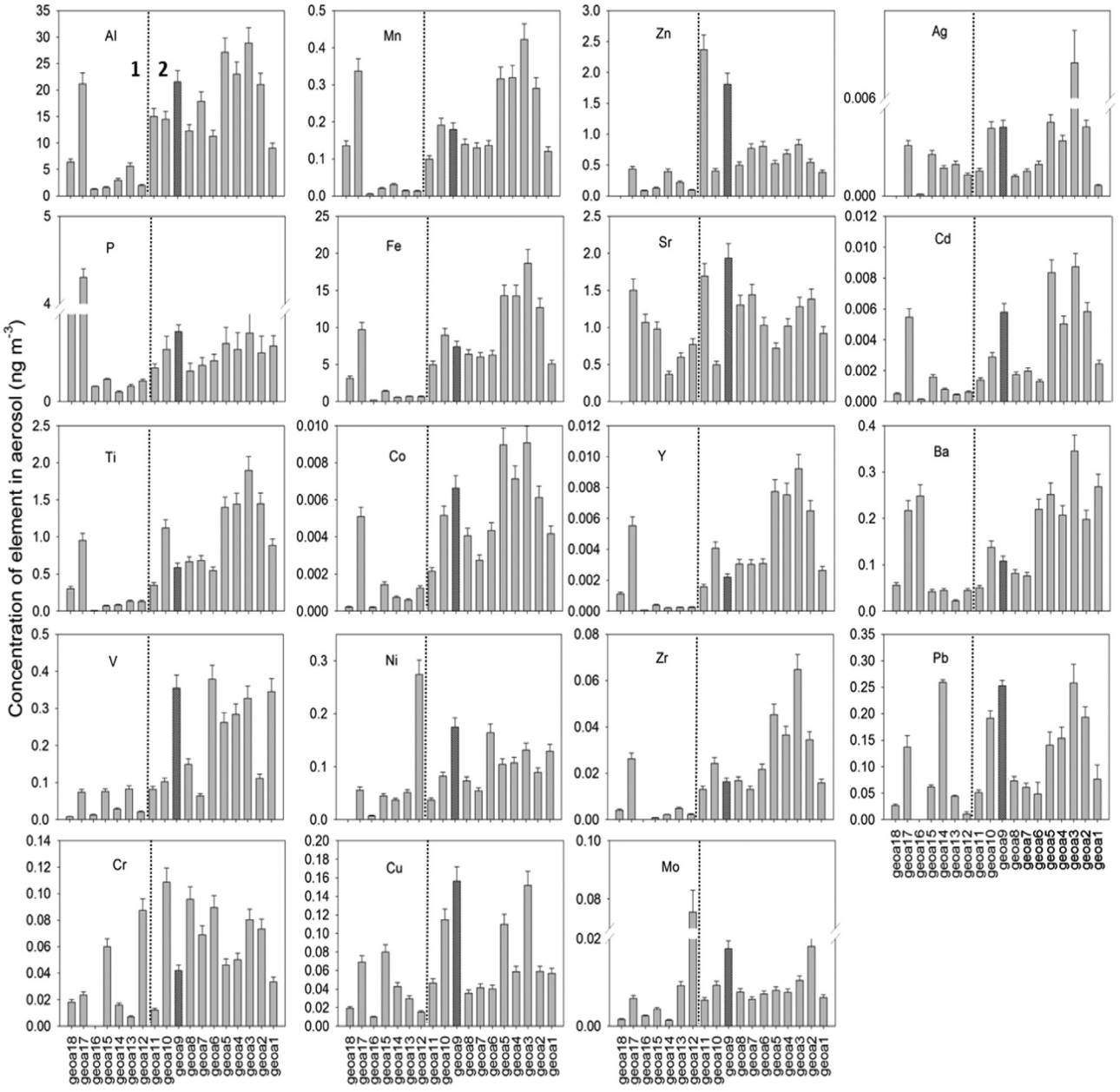

Fig. 2. Aerosol TE concentrations (ng m^{-3}) ± 1SD. The x-axis is reversed to reflect the longitude of the sample locations, i.e. west-east. Sample *geoa*9 is patterned to facilitate identification in these plots, and the boundary between Areas 1 and 2 is marked by a dashed vertical line. The data is displayed in Table S1 (Supplemental Material) and is available on request from the corresponding author or the LEFE-CYBER database (http://www.obsvlfr.fr/proof/php/GEOVIDE/GEOVIDE.php).

In addition to similar spatial distributions, an Fe/Ti elemental mass ratio close to mean UC (10.2 ± 1.1; Rudnick and Gao, 2003) also suggests a common crustal source for these two elements. Indeed, a strong correlation is often observed between Fe and other lithogenic TEs such as Ti in aerosol concentration data (this study, r^2 =0.95, P < 0.001) (Fig. 3A). However, as there is some degree of variability in elemental abundances in crustal material (e.g., 13% and 11% variability for Ti and Fe, respectively; Rudnick and Gao, 2003), mineral dust source materials can have elemental ratios that significantly differ from the UC mean. In this study, the average (± 1 SD) Fe/Ti mass ratio was 10.5 ± 4.5 (Table S4, Supplemental Material), which does not vary significantly from the mean UC ratio, although the range was large (5.0–22.0; Fig. 3B, Table S4). This situation could be due to non-lithogenic inputs of Ti where the ratio was low, and non-lithogenic inputs of Fe where the ratio was high (i.e. variations in the Fe/Ti ratios in the source material). It is less likely to be due to depletion of one metal with respect to the other during atmospheric transport and deposition.

Given the distance covered, from Portugal to Greenland to Newfoundland (approximately 6000 km), it is not hard to imagine that different mineral phases would comprise the bulk aerosol in different parts of the North Atlantic basin, and that these would be reflected by differences in the elemental ratios. Indeed, the Fe/Ti ratios fall into four loose groups: (1) Newfoundland shelf =10.3 ± 0.2 (*geoa*17–18, longitudes > 48°W); (2) Labrador Sea =20.7 ± 1.8 (*geoa*15–16); (3) SW Irminger Sea =5.7 ± 1.1 (*geoa*12–14); and (4) Area 2=9.9 ± 2.3 (*geoa*1–11). There is more variability (RSD ~20%) in the third and fourth groups than the other two groups, but none of the ratios were identified as outliers by a Grubb's test at the 95% confidence level. However, samples *geoa*9 and 11 had relatively high Fe/Ti ratios (13 and 14 respectively), and air mass back trajectories over the UK (Fig. S1, Supplemental Material), which suggests that industrial emission aerosols produced in the UK/western Europe could have become entrained with mineral dust, thus driving the Fe/Ti ratio up.

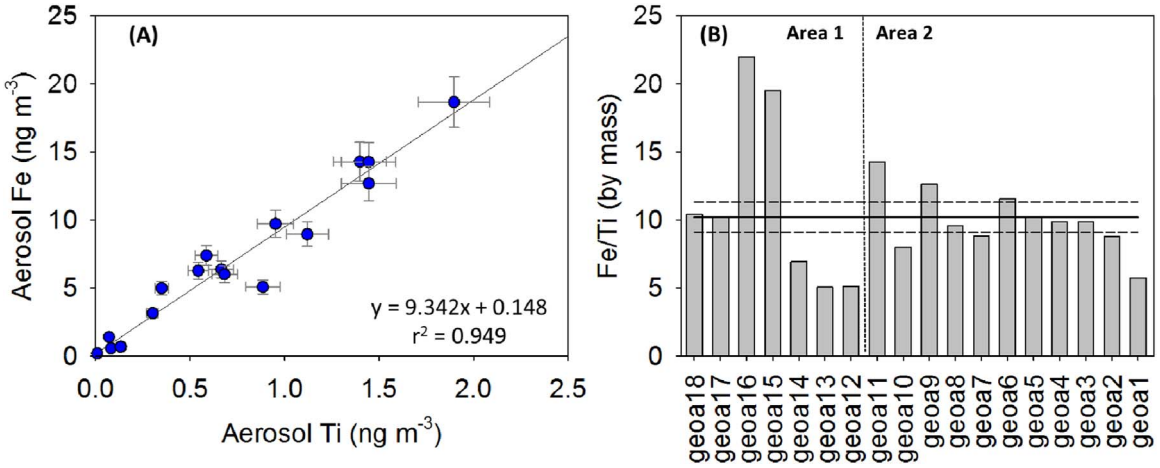

Fig. 3. The linear relationship between aerosol Fe and Ti (A), the mass ratio of Fe/Ti (B), the solid horizontal line represents the mean mass ratio in UC of 10.2 ± 1.1 (± 1SD is indicated by the horizontal dashed lines; Rudnick and Gao, 2003).

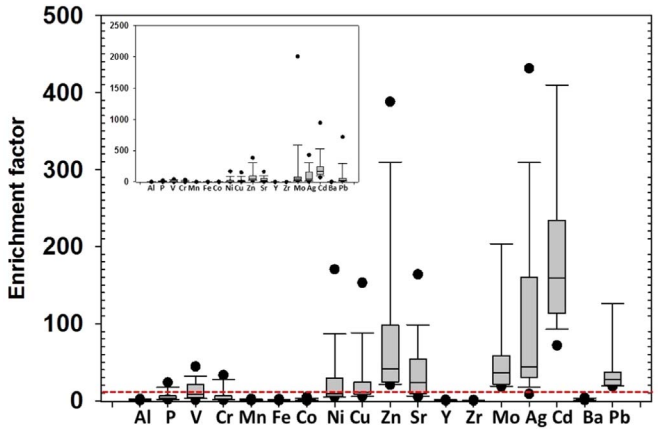

Fig. 4. Box and whisker plots of enrichment factors (EFs; normalised to Ti). Outliers are marked with black dots, and the line in the box is the median value. The inset plot includes all data, except sample *geao*16. The main plot excludes the three EFs > 500 (Mo, Cd and Pb). The red dashed line indicates an EF of 10; data above this line are considered significantly enriched.

TEs are frequently enriched in industrial emission aerosols compared with natural crustal abundances (e.g. Gelado-Caballero et al., 2012). Enrichment factors (EFs) are calculated by dividing the ratio of a TE to a lithogenic tracer (e.g. TE/Ti) in the sample by the same ratio in a reference crustal material (e.g. upper crust, Rudnick and Gao, 2003). In this way, EFs may be used to suggest whether aerosol TEs are sourced from mineral dust or from anthropogenic activities, such as metal smelting or fossil fuel combustion. Due to the natural variability of TE abundance in crustal material we only consider EFs > 10 as significantly enriched. As expected, the primarily lithogenic TEs, Al, Mn, Fe, Co, Y, Zr and Ba, had EFs < 10 for all samples. Mixed-sourced TEs (those having mineral dust, and anthropogenic sources) had median EFs < 10 (3.4, 8.2, and 2.4 for P, V and Cr, respectively), plus 2–5 samples with EFs > 10. Ni and Cu also had median values close to 10 (8.8 and 11, respectively), so can also be described as mixed-source here. The remaining TEs, Zn, Sr, Mo, Ag, Cd and Pb, all had median values > 10, and with the exception of Sr and Ag, no samples with EFs < 10 (Fig. 4). With the exception of Sr, this group of elements are likely to be primarily derived from pollution sources. Vitousek et al. (1999) argue that most aerosol Sr over the open ocean is sourced by sea salt. However, Sr in seawater is 10^6 more abundant than Ti (i.e. μmol kg^{-1}, compared to pmol kg^{-1}) (de Villiers, 1999; Dammshäuser et al., 2013), which results in an elemental mass ratio seven orders of magnitude higher than the crustal ratio. Given that the range of Sr/Ti EFs in this study was 5.3–164, the EFs suggest that the dominant source of Sr was terrestrial, with sea salt likely contributing in the case of significant enrichment. This is consistent with the observation that the Sr/Ti ratios were generally lower (with the exception of *geoa*10) closer to continental landmasses (Table S4, Supplemental Material).

3.3. Positive matrix factorisation (PMF)

The use of PMF was explored as an alternative to enrichment factors for categorising aerosol source apportionment. The EPA-PMF output suggests that the GEOVIDE aerosol TE data can be described by just two factors (Fig. 5). Factor 1 is dominated by Zr (100% of the variability in the aerosol Zr data is explained by this factor). In addition, > 90% of Ti, Mn, Fe, Ag, and Y, and 88.5% of Al is described by Factor 1. This combination of primarily lithogenic TEs (exception Ag) suggests that Factor 1 represents a mineral dust source. This factor is relatively more dominant early in the cruise close to the Iberian Peninsula (samples *geoa*2–5), and on the Newfoundland shelf (*geoa*17). Factor 2 is dominated by Sr (99.7% of the variability in aerosol Sr is explained by Factor 2), which is also primarily lithogenic, based on the calculated EFs. However, Factor 2 also had high contributions from V, Ni and Cu (72.8%, 76.7% and 73.7%, respectively, and was most important from ~53.4–55.5°N (*geoa*9), so may also have an anthropogenic component given that these four elements all show some degree of enrichment (25, 24, 37 and 40 for V, Ni, Cu and Sr, respectively) at this location. For example, V and Ni are particularly enriched in exhaust emissions from marine engines using heavy fuel oils, and to a lesser extent so are Zn (50% in Factor 2) and

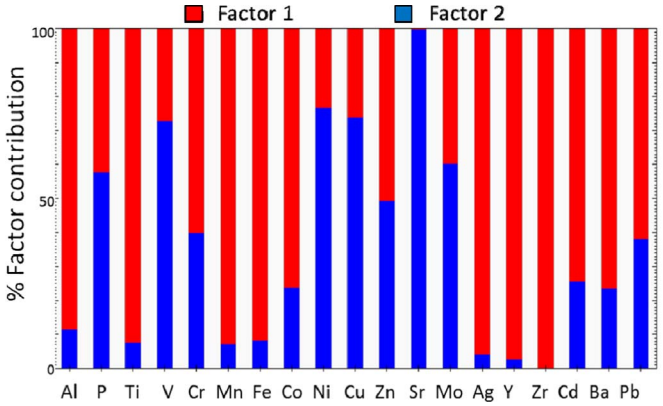

Fig. 5. Factor fingerprint of a two factor model of the aerosol samples from *GEOVIDE* for factor contributions > 0.05%. A factor fingerprint is a stacked bar chart which shows the contribution (in percentage) of each element to the factors.

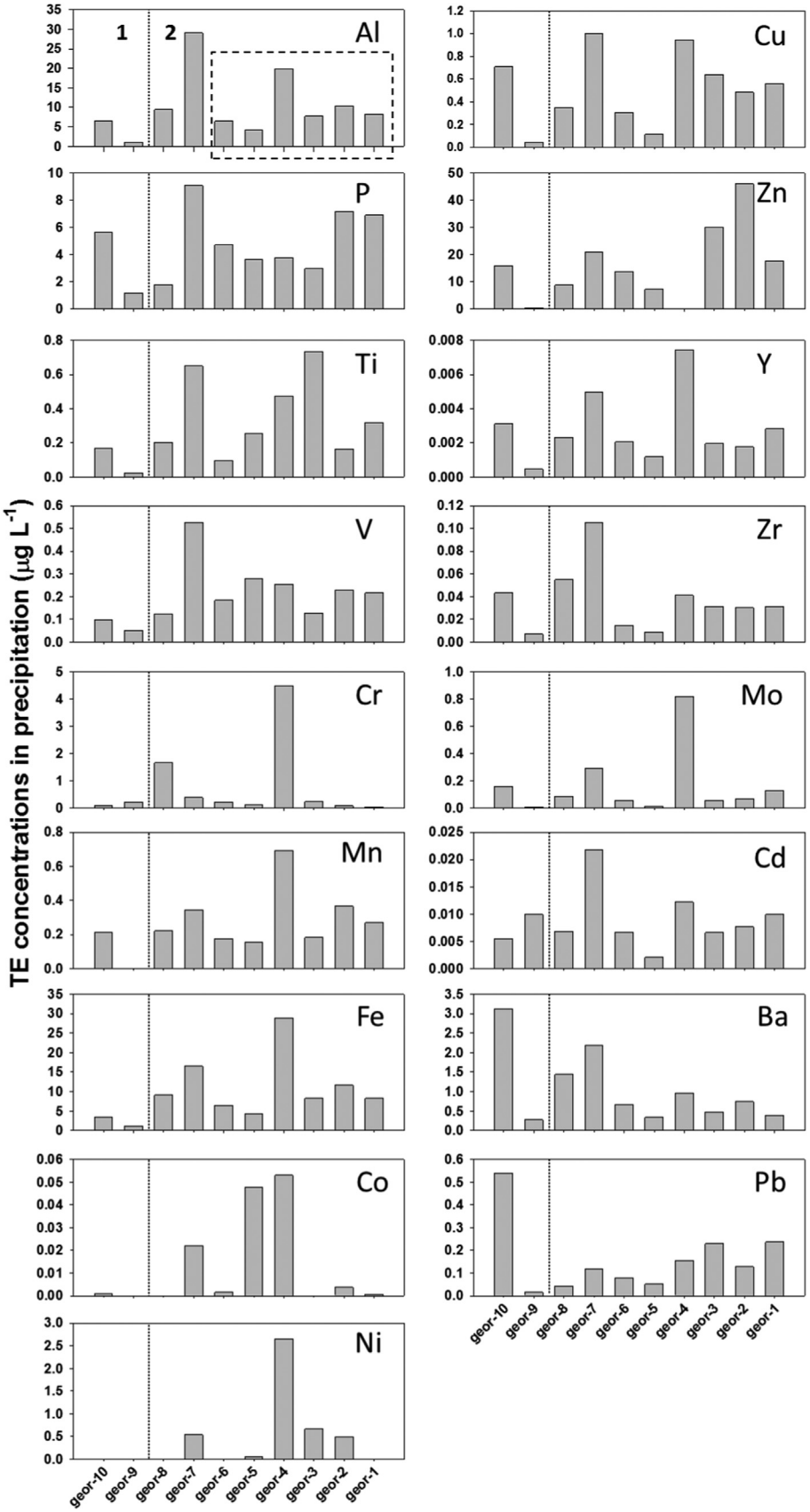

Fig. 6. Rainwater TE concentrations (μg L^{-1}). The x-axis is reversed to reflect the longitude of the sample locations, i.e., west-east. The dotted line marks the boundary between Areas 1 and 2, and the dashed square surrounds samples *geor*1–6, which were collected in approximately the same location over a 36 h period. The full data set is displayed in Table S2 in the Supplemental Material and has been submitted to the LEFE-CYBER database.

Cu (Celo et al., 2015; Streibel et al., 2016). The non-ferrous metal production industry is also an important source of Cu (Pacyna and Pacyna, 2001). In addition, these TEs are also present in mineral dust (e.g. Shelley et al., 2015). Thus, it seems likely that this factor represents a mixed dust source, comprised of a combination of minor crustal elements, sea salt, and industrial emissions from the UK/western Europe and/or shipping emissions. Factor 2 was also relatively more important from 58.2°N 29.7°W–59.1°N 46.1°W (*geoa*11–15) (Fig. S3, Supplemental Material), i.e. furthest from continental Europe and North America, where local sources such as shipping emissions can contribute relatively more to the TE composition of the bulk aerosol.

3.4. Rainwater TE distributions

As is often the case at sea, rain events were infrequent during this study (Fig. 6, n =10), and tended to occur relatively close to land masses. For example, six of the ten rain events (*geor*1–6) occurred early in the study at the same location (40.3°N, 10.0°W), over the course of ~36 h (19–20 May 2014). Sample volumes ranged from 13 to 1100 mL. The sample volume effect (higher concentrations of TEs observed in smaller sample volumes; Jaffrezo et al., 1990) was tested by fitting an exponential decay curve to rain samples *geor*1–6 (assumed to be one extended event), but no significant relationship between sample volume and TE concentrations was observed using this approach (data not shown). As with the aerosol samples, TE concentrations in rainwater were generally low, with the range in TE concentrations being comparable to the aerosol concentrations (Figs. 2 and 6). However, in contrast to the aerosol TE data, the relationship between rainwater Fe and Ti was poor (r^2=0.28), suggesting elemental ratios in rainwater do not reflect crustal ratios. This is likely a result of differences in the solubility of these TEs, as the rain samples were acidified on collection, but unfiltered.

3.5. Atmospheric deposition fluxes

Dry deposition (traditional approach): Marine aerosol samples are collected at sea or from remote island or promontory sites using high or low volume total suspended particulate (TSP) samplers, and dry deposition TE fluxes are estimated from the TE aerosol concentrations multiplied by a dry deposition velocity (V_d; e.g. Duce et al., 1991). The dry deposition fluxes from this study are presented as box and whisker plots to cover the range for each element in the two regions (Areas 1 and 2) either side of 30°W longitude (Fig. 7). As the GEOVIDE aerosol samples were not size-resolved, a V_d of 1.2 cm s^{-1} (Torres-Padrón et al., 2002; Buck et al., 2010) was used for elements with enrichment factors < 10 (primarily lithogenic), and 0.3 cm s^{-1} (Chance et al., 2015) for the remaining elements (Cu, Zn, Mo, Ag, Cd, Pb). As TSP samples are only a snapshot of the aerosol composition at that location, taking a boxed approach in this study allows us to estimate a monthly flux (roughly May 2014 for Area 2, and June 2014 for Area 1). The median fluxes (indicated by the line in the box plots, Fig. 7) were always higher in Area 2 than Area 1 (1.5-11x higher). This was an expected outcome given that the lowest aerosol Ti concentrations, and by implication the lowest aerosol loadings, were observed in Area 1 (Fig. 2). Our dry deposition flux estimates are consistent with those from other low atmospheric deposition regions of the Atlantic Ocean, e.g., 40–68°N (Buck et al., 2010), 40–50°N (Baker et al., 2013), and the southeastern Atlantic (Chance et al., 2015).

Wet deposition (traditional approach): Compared to aerosol chemical composition studies, there are relatively few rain water chemical species composition data. The main reason for this is that rain samples are usually collected at sea on an event basis, by fortuitously being in the right place, at the right time. Precipitation sampling has also occurred on remote island or promontory sites, but sampling stations are typically occupied for shorter periods than aerosol sampling sites due to the challenge of sample storage and collection. In addition, there is an ongoing question regarding bias in rainfall measured at land-based sites relative to the surrounding ocean. Furthermore, the location of the sampling site can also introduce bias, for instance, Kadko and Prospero (2011) demonstrated a consistent offset in sampled volumes between samples collected at two locations and altitudes on the island of Bermuda over a two-year period, despite similar meteorological conditions at both sites.

In some regions of the open ocean wet deposition exceeds dry deposition (Duce et al., 1991), and even in regions where dry deposition dominates over wet deposition, rain during/after a "dust event" could have important local impacts on TE concentrations in surface waters. For all elements in this study, the wet deposition flux in Area 2 exceeded that in Area 1 by 1–85% (Fig. 8; Table S6). For example, the wet deposition flux estimates for Fe were: 2.3 μg m^{-2} d^{-1} (Area 1) and 26 μg m^{-2} d^{-1} (Area 2), an order of magnitude difference. Given that the median Fe dry deposition flux (assuming a V_d of 1.2 cm s^{-1}) was 0.68 μg m^{-2} d^{-1} for Area 1, and 7.4 μg m^{-2} d^{-1} for Area 2, this data suggests that wet deposition dominated the flux of Fe to our study region during May-June 2014. In regions of the Atlantic Ocean where aerosol supply is not dominated by Saharan dust, the wet and dry deposition fluxes of Fe are thought to be roughly equal (e.g., Chance et al., 2015). In contrast, in areas where Saharan dust represents a significant input (e.g., Bermuda, Sholkovitz et al., 2009) dry deposition dominates. The dominance of the wet deposition flux over the dry flux held for all other TEs in the study area, except Al, P and Ti. In Area 1, wet and dry fluxes were roughly equal, but the wet flux of Ti was only half that of the dry flux. In Area 2, the wet and dry fluxes were roughly equal for these three elements.

Total deposition (^{7}Be approach):The measured aerosol ^{7}Be concentrations reported in Table 2a (0.078 ± 0.017–0.35 ± 0.02 dpm m^{-3}) are comparable with the range of the two years of aerosol ^{7}Be concentration data at Station Alert, Canada (0.0090–0.29 dpm m^{-3}; Dibb et al., 1994), a low-dust regime. However, the true range of ^{7}Be concentrations from this study includes lower concentrations as ^{7}Be activity was below detection in all aerosol samples from the Irminger and Labrador Sea regions (Table S2). This latter point is an important limitation to the use of the ^{7}Be technique, but by increasing the volume of air filtered, and as analytical capabilities improve, an issue that might be expected to occur less frequently.

In this study, dry deposition accounted for 9–65% of the total ^{7}Be deposition flux (Table 2a), the remaining 35–91% being supplied by wet deposition, which is less than the 95% observed during a two-year study on Bermuda by Kadko and Prospero (2011). However, the estimation of the balance of the wet to dry deposition flux is dependent on the deposition velocity used in the dry deposition flux calculation. Here, we used 0.3 cm s^{-1} to represent submicron particles, but the Kadko and Prospero study used 0.1 cm s^{-1}. If we were to have used this lower velocity, then wet deposition would have accounted for 78–97% of the total ^{7}Be flux, which is consistent with the 95% reported for Bermuda. Regardless, these data confirm that wet deposition is the primary mode of delivery for ^{7}Be to surface waters (Young and Silker, 1980).

The inventories of ^{7}Be in the water column (Fig. 9) presented in this study (5700–23300 dpm m^{-2}) are comparable in magnitude to those reported by Young and Silker (1980) in the North Atlantic for latitudes greater than 40°N (15000–25000 dpm m^{-2}). According to these authors, inventories of ^{7}Be in the North Atlantic are higher in the western part and particularly in the Sargasso Sea region, and lower in the eastern part, particularly in the Canary region. In fact, inventories of ^{7}Be south of 36°N in the Azores-Canary region (15300–30000 dpm m^{-2}, Kadko and Olson, 1996) and the Sargasso Sea (24800–50500 dpm m^{-2}, Kadko and Prospero, 2011) also show a westward increasing trend. In this study, however, the inventories did not show either south-north or east-west trends. Also, the mean ^{7}Be flux calculated from the water column inventory (160 ± 70 dpm m^{-2} d^{-1}; Table 2b) in this study is 2.9 (± 1.8) times smaller than the mean ^{7}Be

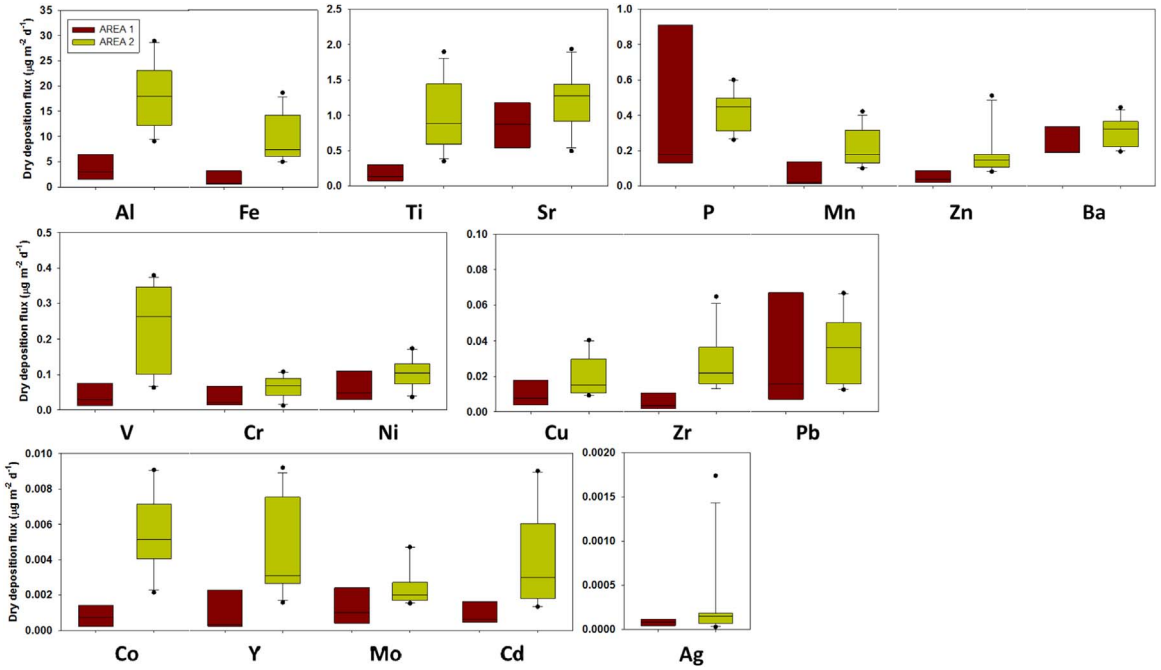

Fig. 7. Dry deposition fluxes for Area 1 (red; west of 30°W, n =7) and Area 2 (green; east of 30°W, n =11). Note the variable y-axes scales. The horizontal line in the box represents the median value, and the boundaries of the box represent the 25th and 75th percentiles. The error bars (whiskers) indicate the 10th and 90th percentiles. Error bars are not displayed for the Area 1 fluxes as the sample population was too small. All data is given in Table S5 (Supplemental Material). (For interpretation of the references to color in this figure legend, the reader is referred to the web version of this article.)

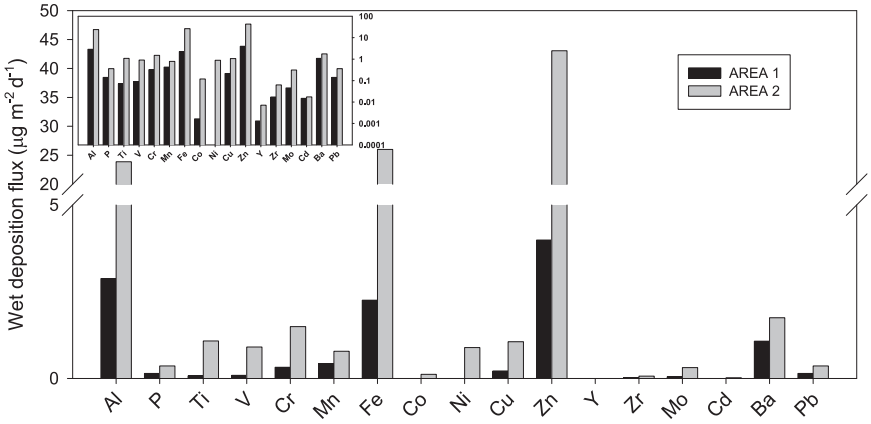

Fig. 8. Wet deposition fluxes for Area 1 (black; west of 30°W) and Area 2 (grey; east of 30°W). Ni was below detection in Area 1. The inset is the same data plotted on a log scale. The data for this plot can be found in Table S6 (Supplemental Material).

flux calculated from precipitation samples (460 ± 210 dpm m^{-2} d^{-1}; Table 2c). There are three possible explanations for this mismatch. Firstly, the ^{7}Be fluxes estimated from the precipitation samples integrate over a short time scale (from 1 to 8 days during the cruise), while ^{7}Be fluxes based on the water column inventories integrate on a seasonal time scale (about 2.5 months prior to the sampling date). Therefore, precipitation samples are more sensitive to changes in the variation of surface air concentrations of ^{7}Be compared to the water column inventories, whereby ^{7}Be is homogenised in the mixed layer and relatively insensitive to fluctuations in atmospheric supply (Kadko and Prospero, 2011). Indeed, surface air concentrations of ^{7}Be peak during the warm season as a consequence, in part, of an increased rate of vertical transport within the troposphere, bringing air enriched in ^{7}Be from higher levels to the surface, especially at middle latitudes (Feely et al., 1989). This would explain, at least partially, the higher ^{7}Be fluxes derived from the precipitation samples with respect to those from the water column inventories, since the former only covered warm months (May/June) while the latter also included colder months (from March to May/June). Also, if it had rained less in the preceding few weeks than it did during the *GEOVIDE* campaign the water column inventories would be lower. However, this does not appear to be the case from the satellite data (Figs. S5 and S6, Supplemental Material). Because of the sensitivity of the precipitation data to fluctuations in atmospheric supply of ^{7}Be, and the time of year of this study, the inventory of ^{7}Be in the upper water column is the preferred choice for calculating ^{7}Be-derived TE fluxes on a seasonal time scale. Secondly, ^{7}Be can be scavenged by particles in coastal environments (e.g., Sommerfield et al., 1999; Venti et al., 2012). Here, in the open ocean, which is characterised by low particle regimes, we assumed that this would be negligible, in accord with the pioneering work of Kadko et al. (2015, 2016). However, we note that phytoplankton blooms were observed at some locations during the cruise. Therefore, the discrepancy may also be a result of the scavenging of ^{7}Be to suspended particles and subsequent sinking to depth. Given that a steady state flux is needed to sustain the seawater inventories shown in Table 2b, and that scavenging of Be by sinking particles is sensitive to the composition of the particles (Chase et al., 2002; Chuang et al., 2015), constraining loss of ^{7}Be via particle scavenging and export deserves

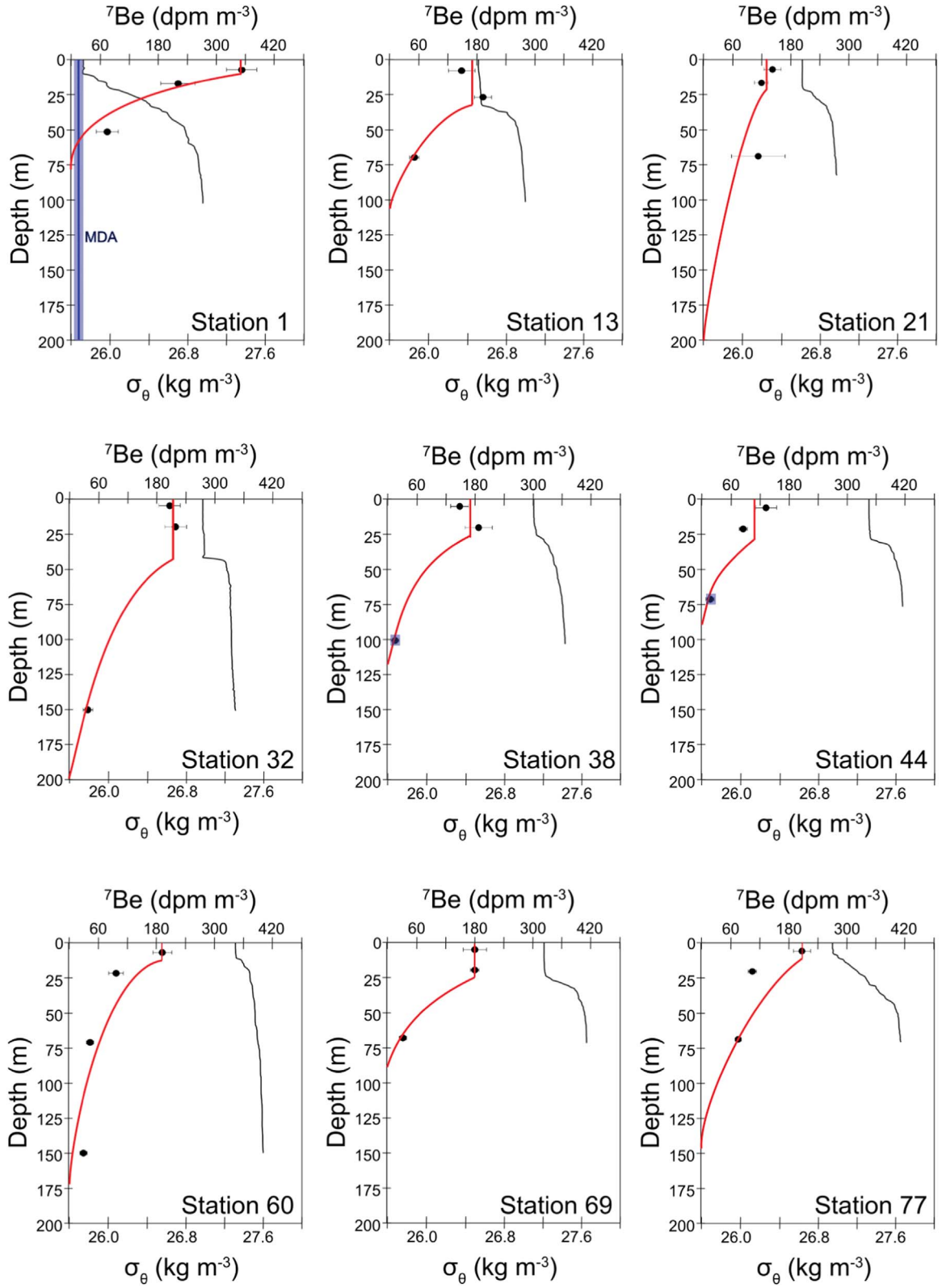

Fig. 9. Concentration profiles (black dots), integrated inventory of ^{7}Be (red continuous line) in the water column and potential density anomaly (σ_θ, black continuous line) for all stations sampled during the GEOVIDE cruise. The Minimum Detectable Activity (MDA) averaged from all ^{7}Be measurements (19 ± 8 dpm m^{-3}) is shown in the panel for Station 1 (shaded blue area). The inventory of ^{7}Be below the mixed layer was calculated using a simple exponential fitting taking into account the concentrations of ^{7}Be at the base of the mixed layer and below. Depths where the fitting-derived ^{7}Be concentration would be 1% of that in the mixed layer are: 77 m (station 1), 106 m (station 13), 199 m (station 21), 211 m (station 32), 116 m (station 38), 83 m (station 44), 167 m (station 60), 94 m (station 69) and 151 m (station 77). For the exponential fitting, average MDA values were assigned to concentrations of ^{7}Be below the MDA found at station 38 (100 m) and station 44 (70 m). At station 21, the exponential fitting led to a clear overestimation of the inventory and predicted the presence of ^{7}Be far below (up to 9000 m) the bottom depth at that station (4467 m). Because this approach led to unreasonable inventories, a new exponential fitting with a fixed slope (averaged from the slopes of the other stations) was used. (For interpretation of the references to color in this figure legend, the reader is referred to the web version of this article.)

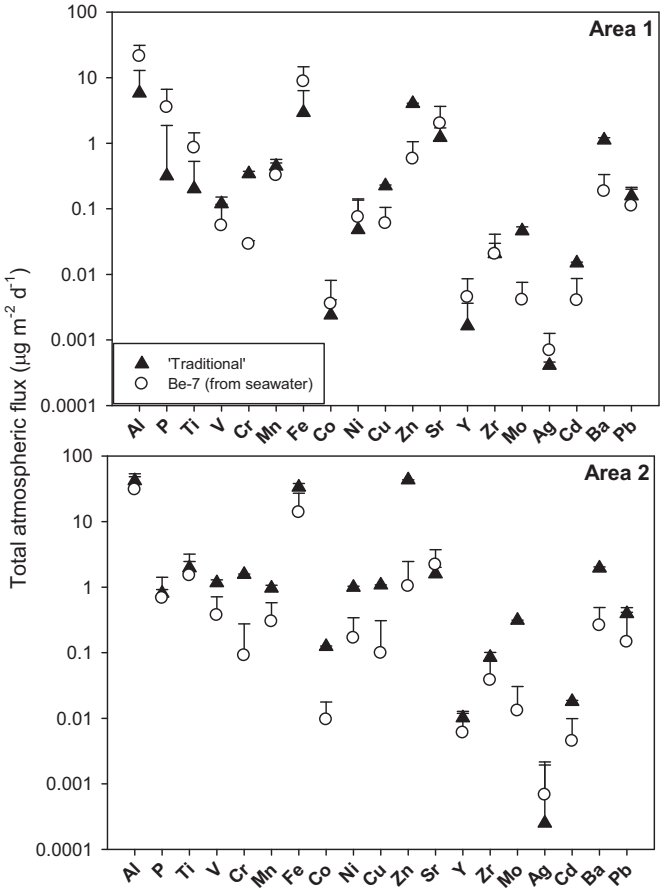

Fig. 10. Comparison of the median TE fluxes (+1 SD) calculated using dry+wet deposition estimates (traditional approach, black triangles), and the ^{7}Be approach using the ^{7}Be inventory in seawater (open circles). Only positive error bars are displayed because negative values cannot be plotted on a log scale. Negative values occur when the SD is greater than the median value. The data for these plots can be found in Table S7 (Supplemental Material).

further investigation, especially in regions where intense phytoplankton blooms occur. Finally, upwelling of ^{7}Be-poor waters can replace ^{7}Be-rich surface waters. Upwelling is favoured by northerly winds, typically from April to September, off the coast off Portugal (Lemos and Pires, 2004). The distribution of temperature and density in the water column off Lisbon did not reveal strong upwelling events during the study. However, because northerly winds were dominant 2–3 months before sampling, some underestimation of the water column inventory of ^{7}Be cannot be ruled out at stations 1 and 13. Consequently, considering the potential effects of scavenging and upwelling, we note that the water column inventories presented in this study provide conservative estimations for the atmospheric fluxes of ^{7}Be, and hence TEs.

3.6. Comparison of flux estimates

In order to assess how total (i.e., dry plus wet) atmospheric fluxes calculated using the traditional approach (Eqs. (1) and (2)), and using the ^{7}Be method (Eq. (7)) compare for the species of interest, the data is plotted for Areas 1 and 2 (Fig. 10).

In Area 1 there was very good agreement for V, Mn, Co, Ni, Sr, Zr and Pb (median values within one positive SD of the lower value). For Cr, Cu, Zn, Mo, Cd and Ba the traditional approach resulted in estimates 3.5–12 times higher. In contrast, for Al, P, Ti, Fe, Y and Ag the ^{7}Be approach resulted in estimates from 2 to 11 times higher. In Area 2 there was very good agreement between flux estimates for Al, P, Ti, Sr, Y, Zr, Ag and Pb, whereas the traditional approach resulted in flux estimates 2–42 times higher for V, Cr, Mn, Fe, Co, Cu, Ni, Zn, Mo, Cd and Ba. There are a couple of points that should be noted. Firstly, the TEs with good agreement between the flux estimates were not the same in the two areas. This could simply be the result of the disparity between the number of samples in each area (only 2 for Area 1, compared to 10 for Area 2), or there could be systematic differences in how TEs are delivered to the surface ocean and their subsequent behaviour in the water column following deposition. Secondly, the traditional approach results in higher median estimates for all TEs (except Ag and Sr) in Area 2 and for six TEs (Cr, Cu, Zn, Mo, Cd and Ba) in Area 1, whereas the ^{7}Be approach yielded higher estimates for a number of lithogenic TEs in Area 1. The possible reasons for this offset are explored and suggestions made for future studies applying these techniques for TE deposition flux estimation.

(i) The two techniques provide estimates on different timescales: The traditional approach provides a snap shot of deposition (and aerosol TE concentrations show significant day-to-day variability), whereas the ^{7}Be technique provides a seasonal estimate for spring (March-April-May-June) 2014. As the inventory of ^{7}Be is a reflection of the mean life-time of ^{7}Be in the water column, and ^{7}Be deposition is lowest in the cooler months prior to the cruise (Young and Silker, 1980; Akata et al., 2008), the ^{7}Be inventories used here most likely encompassed a period of time when ^{7}Be atmospheric inputs were lower than at the time of our field campaign. The impact of the different timescales of integration are best exemplified by the higher ^{7}Be flux estimates derived from precipitation samples compared with the water column inventories. The higher TE flux estimates derived from the traditional approach in several instances, particularly in Area 2, could also be directly related to this temporal mismatch, with aerosol samples representing up to 48 h integrations and the water column inventory, approximately 2.5 months. This is highly relevant for constraining atmospheric deposition on seasonal, or annual, timescales in models.

(ii) Representative dry deposition velocities: Aerosol TEs released by high temperature industrial processes tend to be smaller than lithogenic and sea salt aerosols and, thus, have a smaller V_d (Duce et al. 1991). The uncertainties that the V_d term introduces to the dry deposition flux estimates provide the impetus to find new ways to constrain this term. Constraint of this term requires accurate parameterisation of wind speed, relative humidity and particle type (Slinn and Slinn, 1981). As we do not have data describing the particle size distribution and type for this study, it is challenging to constrain the uncertainties, but it is proposed to be up to a factor of three (Duce et al., 1991). Although we cannot verify the validity of this uncertainty, we can calculate an effective bulk deposition velocity (combined dry and wet aerosol deposition velocity;

Table 3
The effective bulk deposition velocity (± propagated uncertainty) calculated using the ^{7}Be fluxes derived from seawater and aerosol concentrations of ^{7}Be (using Eq. (5)) from samples collected at the same approximate location. Note that there is no data for samples *geoa*11-16, inclusive, as ^{7}Be was below detection in aerosol samples at the time of station occupation.

Area	Aerosol Sample	Water column Station	Bulk V_d m d^{-1}	cm s^{-1}
2	geoa1	1	1900 ± 400	2.2 ± 0.5
2	geoa4	13	610 ± 70	0.71 ± 0.08
2	geoa6	21	2500 ± 400	2.9 ± 0.5
2	geoa9	32	2800 ± 500	3.2 ± 0.6
1	geoa17	69	1330 ± 160	1.54 ± 0.18
1	geoa18	77	2200 ± 300	2.6 ± 0.4
2	Mean (± 1SD)		2000 ± 1000	2.3 ± 1.1
1	Mean (± 1SD)		1800 ± 600	2.0 ± 0.7
1+2	Mean (± 1SD)		1900 ± 800	2.2 ± 0.9

Table 3) from Equation 5 (Kadko et al., 2016), and use it to suggest where wet deposition is likely to be an important factor for the delivery of TEs, and/or where there may be an unaccounted loss term for ^{7}Be (e.g., scavenging in the water column). It should be noted that this approach assumes that a fixed deposition velocity of 1000 m d^{-1} (Duce et al., 1991; Buck et al., 2010) is appropriate for mineral dust deposition in the remote North Atlantic.

Where the bulk deposition velocities displayed in Table 3 are significantly greater than 1000 m d^{-1}, it suggests that wet deposition played a significant role in determining the total TE fluxes, as demonstrated by the calculated wet and dry deposition fluxes (Figs. 7 and 8). With the exception of sample *geoa*4 (Station 13), this was the case throughout the cruise. While rain events were infrequently sampled, humidity was generally > 90% and thick fog was frequently encountered between 27 May 2014 (*geoa*5) and 25 June 2014 (*geoa*17). Values close to or less than 1000 m d^{-1} suggest that there is a loss term missing from our equations, or that the aerosol size distribution was dominated by fine mode, sub-micron particles with lower dry deposition velocities. However, as internal mixing with sea salt aerosols leads to some degree of homogenisation in the size distribution of remote marine aerosols (Andreae et al., 1986) this explanation is doubtful, but could be tested with a size-resolved aerosol sampling strategy.

(i) The assumption of negligible scavenging of ^{7}Be onto sinking particles may be incorrect: Bearing in mind that the study region is an area subject to intense phytoplankton blooms during spring (the season of the present study), and that Be has an affinity for a variety of particle types (Chase et al., 2002; Chuang et al., 2015), neglecting this term may result in an underestimation of the TE fluxes using the ^{7}Be approach. Indeed, the effective bulk deposition calculations suggest that for some stations water column scavenging of ^{7}Be could have been significant. Particle scavenging during this study will be the subject of a separate manuscript (N. Lemaitre et al., in prep), and future studies using the ^{7}Be approach should aim to quantify and parameterise scavenging of ^{7}Be onto sinking particles.

(ii) Representative precipitation rates: The precipitation rate term is the largest source of uncertainty in wet deposition flux calculations, as it can be challenging to determine accurate values in remote marine regions (e.g., Chance et al., 2015). In this study, the precipitation rates used were based on averages retrieved from satellite products (TRMM and GPM from Giovanni). Precipitation rates determined from field sampling can be inaccurate due to the confounding influence of sea spray, variable wind speeds and no splash screens on the samplers, and in some regions (although not applicable to this study), evaporation. As such the parameterisation of precipitation rate most certainly introduced errors to the calculation of the dry + wet flux (black triangles in Fig. 10). We are reluctant to quantify this uncertainty without having explicitly tested for it. However, by comparing the precipitation rate of 2 mm d^{-1} used for the wet flux calculations with the range of precipitation rates determined from field collections (2 –7 mm d^{-1}) we hypothesise that an error of three to fourfold is not unreasonable. For the ^{7}Be approach the issue of precipitation rate is avoided by using the ^{7}Be inventory in seawater rather than ^{7}Be concentrations from precipitation samples, as the former is less impacted by short-term fluctuations in ^{7}Be inputs.

In reality, a combination of several, or all, of the above points likely contributes to the variability in the TE flux estimates. The motivation for making comparisons between these two approaches for TE flux estimation is driven by the knowledge that one of the biggest challenges currently faced in aerosol studies is converting aerosol chemical concentration data into realistic flux estimates (Anderson et al., 2016). From this study we are confident that ^{7}Be can be successfully used as a tracer of the atmospheric flux of TEs to the surface ocean in diverse oceanographic settings, particularly where precipitation sampling is either not possible, or is unlikely to be representative. However, effective bulk deposition velocities ≤1000 m d^{-1} suggest that there could be regions where the ^{7}Be approach should be used with caution, such as in particulate-rich open ocean regimes. As such, it would be advisable to continue to test the underlying assumptions of the ^{7}Be approach in order to reduce uncertainties in the deposition flux estimates.

4. Conclusions

Atmospheric deposition of TEs to the study region was low throughout May-June 2014, and particularly low in the Irminger and Labrador Seas, as suggested by the aerosol Ti concentrations (range: 0.0084–1.9 ng m^{-3}). Despite the cruise track of *GEOVIDE* being located north of the extent of the Saharan dust plume, the positive matrix factorisation (PMF) output indicated that the data could be reduced to only two factors, suggesting that the aerosol TE composition could be represented as simply the mixing of two aerosol sources (1=mineral dust, and 2=mixed mineral dust-sea salt-anthropogenic aerosols), largely controlled by the proximity to major land masses.

Trace element deposition fluxes (in particular, Fe) are a key component of ocean biogeochemical models, due to the link between TE supply and the biological carbon pump, yet remain poorly constrained as flux estimates are subject to relatively large uncertainties. Here, we investigated the use of ^{7}Be as a tracer of atmospheric inputs. The TE flux estimates obtained by using the ^{7}Be proxy and the traditional approach (dry + wet deposition) were in excellent agreement for approximately half the TEs investigated, but there were large offsets for other TEs (up to 40x). While our results suggest that the ^{7}Be approach continues to show promise in this application, particularly in regions where precipitation samples cannot be routinely collected, it is important to consider factors such as the timescale of integration, selection of representative deposition velocities and precipitation rates, and particle scavenging and export of ^{7}Be from the mixed layer. As such, the underlying assumptions of the ^{7}Be approach should be examined closely to assess their validity in the region of interest. Work continues to this end. In the meantime, our data provide seasonal TE deposition fluxes for the key *GEOTRACES* elements, and more, for the North Atlantic Ocean (> 40°N) that can be used to help constrain aerosol TE deposition models.

Acknowledgements

Many thanks to the captain and crew of the N.O. Pourquoi Pas? for their help during the *GEOVIDE* mission. Very big “thank you” also goes to Alex Baker (UEA), for the loan of the aerosol sampler used during this project, and to Yi Tang for helping with ^{7}Be sample collections. This work was funded by a LabEX MER International Postdoctoral Fellowship to RUS, grant number ANR-13-B506-0014 to GS, and was partly supported by the Generalitat de Catalunya to the research group MERS (2014 SGR-1356). MRM and MC were supported by Spanish Ph.D. FPU Fellowships (AP2010-2510 and AP2012-2901, respectively). The WHOI postdoctoral scholar VS was supported by the Center for Marine and Environmental Radioactivity (CMER). Trace element determination was conducted at the Pôle de Spectrométrie Océan at the Institut Universitaire Européen de la Mer with the support and guidance of Claire Bollinger and Marie-Laure Rouget. Determination of ^{7}Be was conducted at the Universitat Autònoma de Barcelona with the help of Sarah Paradis, and at the underground laboratory at Ferrières (LAFARA, French Pyrénées). We thank Marc Souhaut for his help at the LAFARA underground laboratory. We are grateful to EDF (Electricité De France) for allowing us to run our germanium detectors in the tunnel of Ferrières. We thank Europe and

Région Occitanie Pyrénées-Méditerranée for supporting the LAFARA underground laboratory through a FEDER funding (SELECT project). We also thank the three anonymous reviewers for their invaluable inputs, and acknowledge the NOAA Air Resources Laboratory (ARL) for the provision of the HYSPLIT transport and dispersion model and/or READY website (http://www.ready.noaa.gov) used in this publication.

Appendix A. Supporting information

Supplementary data associated with this article can be found in the online version at doi:10.1016/j.dsr.2016.11.010.

References

Akata, N., Kawabata, H., Hasegawa, H., Sato, T., Chikuchi, Y., Kondo, K., Hisamatsu, S., Inaba, J., 2008. Total deposition velocities and scavenging ratios of 7be and 210Pb at Rokkasho, Japan. J. Radioanal. Nucl. Chem. 277, 347–355.

Anderson, R.F., Cheng, H., Edwards, R.L., Fleisher, M.Q., Hayes, C.T., Huang, K.F., Kadko, D., Lam, P.J., Landing, W.M., Lao, Y., Lu, Y., Measures, C.I., Morton, P.L., Moran, S.B., Robinson, L.F, Shelley, R.U., 2016. How well do we quantify dust deposition to the ocean? Philos. Trans. R. Soc. A. http://dx.doi.org/10.1098/rsta.2015.0285.

Andreae, M.O., Charlson, R.J., Bruynseels, F., Storms, H., van Grieken, R., Maenhaut, W., 1986. Internal mixture of sea salt, silicates, and excess sulfate in marine aerosols. Science 232, 1620–1623.

Baker, A.R., Adams, C., Bell, T.G., Jickells, T.D., Ganzeveld, L., 2013. Estimation of atmospheric nutrient inputs to the Atlantic Ocean from 50N to 50 S based on large-scale filed sampling: iron and other dust-associated elements. Glob. Biogeochem. Cycles 27, 755–767.

Baker, A.R., Jickells, T.D., Biswas, K.F., Weston, K., French, M., 2006. Nutrients in atmospheric aerosol particles along the Atlantic Meridional Transect. Deep Sea Res. 53, 1706–1719.

Baker, A.R., Lesworth, T., Adams, C., Jickells, T.D., Ganzeveld, L., 2010. Estimation of atmospheric nutrient inputs to the Atlantic Ocean from 50°N to 50°S based on large-scale field sampling: fixed nitrogen and dry deposition of phosphorus. Glob. Biogeochem. Cycles, 24. http://dx.doi.org/10.1029/2009gb003634.

Buck, C.S., Landing, W.M., Resing, J.A., Measures, C.I., 2010. The solubility and deposition of aerosol Fe and other trace elements in the North Atlantic Ocean: observations from the A16N CLIVAR/C_O2 repeat hydrography section. Mar. Chem. 120, 57–70.

Cámara-Mor, P., Masque, P., Garcia-Orellana, J., Kern, S., Cochran, J.K., Hanfland, C., 2011. Interception of atmospheric fluxes by Arctic sea ice: evidence from cosmogenic ^{7}Be. J. Geophys. Res. Oceans 116, 1–10. http://dx.doi.org/10.1029/2010JC006847.

Celo, V., Dabek-Zlotorzynska, E., McCurdy, M., 2015. Chemical characterization of exhaust emissions from selected Canadian marine vessels: the case of trace metals and lanthanoids. Environ. Sci. Technol. 49, 5220–5226.

Chance, R., Jickells, T.D., Baker, A.R., 2015. Atmospheric trace metal concentrations, solubility and deposition fluxes in remote marine air over the south-east Atlantic. Mar. Chem. 177, 45–56. http://dx.doi.org/10.1016/j.marchem.2015.06.028.

Chase, Z., Anderson, R.F., Fleisher, M.Q., Kubik, P.W., 2002. The influence of particle composition and particle flux on scavenging of Th, Pa and Be in the ocean. Earth Planet. Sci. Lett. 204, 215–229.

Cheize, M., Sarthou, G., Croot, P., Bucciarelli, E., Baudoux, A.-C., Baker, A., 2012. Iron organic speciation determination in rainwater using cathodic stripping voltammetry. Anal. Chim. Acta 726, 45–54.

Chuang, C.-Y., Santschi, P.H., Xu, C., Jiang, Y., Ho, Y.-F., Quigg, A., Guo, L., Hatcher, P.G., Ayranov, M., Schumann, D., 2015. Molecular level characterization of diatom-associated biopolymers that bind ^{234}Th, ^{233}Pa, ^{210}Pb, and ^{7}Be in seawater: a case study with Phaeodactylum tricornutum. J. Geophys. Res. Biogeosci. 120, 1858–1869.

Comero, S., Gawlik, B.M., and Capitani, L. 2009. Positive Matrix Factorisation (PMF): an introduction to the chemometric evaluation of environmental monitoring data using PMF. JRC Scientific and Technical Reports. Available at: ⟨http://publications.jrc.ec.europa.eu/repository/bitstream/JRC52754/reqno_jrc52754_final_pdf_version%5B1%5D.pdf⟩, (accessed 24.03.16).

d'Almeida, G.A., 1986. A model for Saharan dust transport. J. Clim. Appl. Meteor. 24, 903–916.

Dammshäuser, A., Wagener, T., Garbe-Schönberg, D., Croot, P.L., 2013. Particulate and dissolved aluminum and titanium in the upper water column of the Atlantic Ocean. Deep Sea Res. 73, 127–139.

de Villiers, S., 1999. Seawater strontium and Sr/Ca variability in the Atlantic and Pacific oceans. Earth Planet. Sci. Lett. 171, 623–634.

Dibb, J.E., Meeker, L.D., Finkel, R.C., Southon, J.R., Caffee, M.W., 1994. Estimation of stratospheric input to the Arctic troposphere: ^{7}Be and ^{10}Be in aerosols at Alert, Canada. J. Geophys. Res. 99, 12855–12864.

Doherty, O.M., Riemer, N., Hameed, S., 2012. Control of Saharan mineral dust transport to Barbados in winter by the Intertropical Convergence Zone over West Africa. J. Geophys. Res. Atmos., 117. http://dx.doi.org/10.1029/2012JD017767.

Duce, R.A., Liss, P.S., Merrill, J.T., Atlas, E.L., Buat-Menard, P., Hicks, B.B., Miller, J.M., Prospero, J.M., Arimoto, R., Church, T.M., Ellis, W., Galloway, J.N., Hansen, L., Jickells, T.D., Knap, A.H., Reinhardt, K.H., Schneider, B., Soudine, A., Tokos, J.J., Tsunogai, S., Wollast, R., Zhou, M., 1991. The atmospheric input of trace species to the world ocean. Glob. Biogeochem. Cycles 5, 193–259.

Feely, H.W., Larsen, R.J., Sanderson, C.G., 1989. Factors that cause seasonal variations in Beryllium-7 concentrations in surface air. J. Environ. Radioact. 9, 223–249.

Ganzeveld, L., Lelieveld, J., Roelofs, G.-J., 1998. A dry deposition parameterization for sulfur oxides in a chemistry and general circulation model. J. Geophys. Res. Atmos. 103, 5679–5694.

Gelado-Caballero, M.D., López-García, P., Prieto, S., Patey, M.D., Collado, C., Hérnández-Brito, J.J., 2012. Long-term aerosol measurements in Gran Canaria, Canary Islands: particle concentration, sources and elemental composition. J. Geophys. Res. Atmos., 117. http://dx.doi.org/10.1029/2011jd016646.

Jaffrezo, J.L., Colin, J.L., Gros, J.M., 1990. Some physical factors influencing scavenging ratios. Atmos. Environ. A-Gen. 24, 3073–3083. http://dx.doi.org/10.1016/0960-1686(90)90486-7.

Jickells, T.D., An, Z.S., Andersen, K.K., Baker, A.R., Bergametti, G., Brooks, N., Cao, J.J., Boyd, P.W., Duce, R.A., Hunter, K.A., Kawahata, H., Kubilay, N., laRoche, J., Liss, P.J., Mahowald, N., Prospero, J.M., Ridgwell, A.J., Tegen, I., Torres, R., 2005. Global iron connections between desert dust, ocean biogeochemistry and climate. Science 308, 67–71.

Jickells, T.D., Spokes, L., 2001. Atmospheric iron inputs to the ocean. In: Turner, D.A., Hunter, K.A. (Eds.), The Biogeochemistry of Iron in Seawater. John Wiley, Hoboken, N.J., 85–121.

Kadko, D., Olson, D., 1996. Be-7 as a tracer of surface water subduction and mixed layer history. Deep Sea Res. 43, 89–116.

Kadko, D., Prospero, J.P., 2011. Deposition of ^{7}Be to Bermuda and the regional ocean: environmental factors affecting estimates of atmospheric flux to the ocean. J. Geophys. Res., 116. http://dx.doi.org/10.1029/2010JC006629.

Kadko, D., Galfond, B., Landing, W.M., Shelley, R.U., 2016. Determining the pathways, fate and flux of atmospherically derived trace elements in the Arctic Ocean/ Ice system. Mar. Chem. 182, 38–50.

Kadko, D., Landing, W.M., Shelley, R.U., 2015. A novel tracer technique to quantify the atmospheric flux of trace elements to remote ocean regions. J. Geophys. Res. Oceans. http://dx.doi.org/10.1002/2014JC010314.

Law, C.S., Breviere, E., de Leeuw, G., Garcon, V., Guieu, C., Kieber, D.J., Kontradowitz, S., Paulmier, A., Quinn, P.K., Saltzman, E.S., Stefels, J., von Glasow, R., 2013. Evolving research directions in Surface Ocean-Lower Atmosphere (SOLAS) science. Environ. Chem. 10, 1–16.

Lemos, R.T., Pires, H.O., 2004. The upwelling regime off the west portuguese coast, 1941–2000. Int. J. Climatol. 24, 511–524.

Monterey, G., and Levitus, S., 1997. Seasonal variability of mixed layer depth for the world ocean. NOAA Atlas, NESDIS, 14, Washington, D.C., 96 pp.

Moore, C.M., Mills, M.M., Arrigo, K.R., Berman-Frank, I., Bopp, L., Boyd, P.W., Galbraith, E.D., Geider, R.J., Guieu, C., Jaccard, S.L., Jickells, T.D., La Roche, J., Lenton, T.M., Mahowald, N.M., Maranon, E., Marinov, I., Moore, J.K., Nakatsuka, T., Oschlies, A., Saito, M.A., Thingstad, T.F., Tsuda, A., Ulloa, O., 2013. Processes and patterns of oceanic nutrient limitation. Nat. Geosci. 6, 701–710.

Morel, F.M.M., Price, N.M., 2003. The biogeochemical cycles of trace metals in the oceans. Science 300, 944–947.

Morton, P.L., Landing, W.M., Hsu, S.-C., Milne, A., Aguilar-Islas, A.M., Baker, A.R., Bowie, A.R., Buck, C.S., Gao, Y., Gichuki, S., Hastings, M.G., Hatta, M., Johansen, A.M., Losno, R., Mead, C., Patey, M.D., Swarr, G., Vandermark, A., Zamora, L.M., 2013. Methods for the sampling and analysis of marine aerosols: results from the 2008 GEOTRACES aerosol intercalibration experiment. Limnol. Oceanogr. Methods 11, 62–78.

Moulin, C., Lambert, C.E., Dulac, F., Dayan, U., 1997. Control of atmospheric export of dust from North Africa by the North Atlantic Oscillation. Nature 387, 691–694.

Nair, P.R., Parameswaran, K., Abraham, A., Jacob, S., 2005. Wind-dependence of sea-salt and non-sea-salt aerosols over the oceanic environment. J. Atmos. Solar-Terr. Phys. 67, 884–898.

Pacyna, J.M., Pacyna, E.G., 2001. An assessment of global and regional emissions of trace metals to the atmosphere from anthropogenic sources worldwide. Environ. Rev. 9, 269–298.

Prospero, J.M., Carlson, T.N., 1972. Vertical and areal distribution of Saharan dust over the Equatorial North Atlantic Ocean. J. Geophys. Res. 77, 5255–5265.

Prospero, J.M., Collard, F.-X., Molinie, J., Jeannot, A., 2014. Characterizing the annual cycle of African dust transport to the Caribbean Basin and South America and its impact on the environment and air quality. Glob. Biogeochem. Cycles 29, 757–773.

Rolph, G.D., 2016. Real-time Environmental Applications and Display System (READY). NOAA Air Resources Laboratory, Silver Spring, MD, Website⟨http://ready.arl.noaa.gov⟩.

Rudnick, R.L., Gao, S., 2003. Composition of the continental crust. In: Holland, H.D., Turekian, K.K. (Eds.), Treatise on Geochemistry. Elsevier, Oxford, 1–64.

Saito, M.A., Goepfert, T.J., Ritt, J.T., 2008. Some thoughts on the concept of colimitation: three definitions and the importance of bioavailability. Limnol. Oceanogr. 53, 276–290.

Schlosser, C., Klar, J.K., Wake, B.D., Snow, J.T., Honey, D.J., Woodward, E.M.S., Lohan, M.C., Achterberg, E.A., Moore, C.M., 2013. Seasonal ITCZ migration dynamically controls the location of the (sub)tropical Atlantic biogeochemical divide. PNAS. http://dx.doi.org/10.1073/pnas.1318670111.

Shelley, R.U., Morton, P.L., Landing, W.M., 2015. Elemental ratios and enrichment factors in aerosols from the US-GEOTRACES North Atlantic transects. Deep Sea Res. 116, 262–272.

Sholkovitz, E., Sedwick, R., P.N, Church, T.M., 2009. Influence of anthropogenic combustion emissions on the deposition of soluble aerosol iron to the ocean:

empirical estimates for island sites in the North Atlantic. Geochim. Cosmochim. Acta 73, 3981–4003.
Sieck, L.C., Burges, S.J., Steiner, M., 2007. Challenges in obtaining reliable measurements of point rainfall. Water Resour. Res., 43. http://dx.doi.org/10.1029/2005WR004519.
Silker, W.B., 1972. Beryllium-7 and fission products in the Geosecs II water column and applications of their oceanic distributions. Earth Plan. Sci Lett. 16, 131–137.
Slinn, S.A., Slinn, W.G.N., 1981. Predictions for particle deposition on natural waters. Atmos. Environ. 14, 1013–1016.
Sommerfield, C.K., Nittrouer, C.A., Alexander, C.R., 1999. ^{7}Be as a tracer of flood sedimentation on the northern California continental margin. Cont. Shelf Res. 19, 335–361. http://dx.doi.org/10.1016/S0278-4343(98)00090-9.
Stein, A.F., Draxler, R.R., Rolph, G.D., Stunder, B.J.B., Cohen, M.D., Ngan, F., 2015. NOAA's HYSPLIT atmospheric transport and dispersion modeling system. Bull. Am. Meteor. Soc. 96, 2059–2077. http://dx.doi.org/10.1175/BAMS-D-14-00110.1.
Streibel, T., Schnelle-Kreis, J., Czech, H., Harndorf, H., Jakobi, G., Jokiniemi, J., Karg, E., Lintelmann, J., Matuschek, G., Michalke, B., Müller, L., Orasche, J., Passig, J., Radischat, C., Rabe, R., Reda, A., Rüger, C., Schwemer, T., Sippula, O., Stengel, B., Sklorz, M., Torvela, T., Weggler, B., Zimmermann, R., 2016. Aerosol emissions of a ship diesel engine operated with diesel fuel or heavy fuel oil. Environ. Sci. Poll. Res., 1–16. http://dx.doi.org/10.1007/s11356-016-6724-z.
Stuut, J.-B., Zabel, M., Ratmeyer, V., Helmke, P., Schefuß, E., Lavik, G., Schneider, R., 2005. Provenance of present-day eolian dust collected off NW Africa. J. Geophys. Res., 110. http://dx.doi.org/10.1029/2004JD005161.
Sunda, W.G., 2012. Feedback interactions between trace metal nutrients and phytoplankton in the ocean. Front. Microbiol., 3. http://dx.doi.org/10.3389/fmicb.2012.00204.
Thomson, R.E., Fine, I.V., 2003. Estimating mixed layer depth from oceanic profile data. J. Atmos. Ocean. Technol. 20, 319–329. http://dx.doi.org/10.1175/1520-0426(2003)020 < 0319:EMLDFO > 2.0.CO;2.
Torres-Padrón, M.E., Gelado-Caballero, M.D., Collado-Sánchez, C., Siruela-Matos, V.F., Cardona-Castellano, P.J., Hernández-Brito, J.J., 2002. Variability of dust inputs to the CANIGO zone. Deep Sea Res. 49, 3455–3464.
van Beek, P., Souhaut, M., Lansard, B., Bourquin, M., Reyss, J.L., von Ballmoos, P., Jean, P., 2013. LAFARA: a new underground laboratory in the French Pyrénées for ultra low-level gamma-ray spectrometry. J. Env. Radioact. 116, 152–158.
Venti, A., Kadko, D., Andersson, A.J., Langdon, C., Bates, N.R., 2012. A multi-tracer model approach to estimate reef water residence times. Limnol. Oceanogr. Methods 10, 1078–1095. http://dx.doi.org/10.4319/lom.2012.10.1078.
Vitousek, P.M., Kennedy, M.J., Derry, L.A., Chadwick, O.A., 1999. Weathering versus atmospheric sources of strontium in ecosystems on young volcanic soils. Oecologia 121, 255–259.
Winkler, R., Dietl, F., Frank, G., Tschiersch, J., 1998. Temporal variation of ^{7}Be and ^{210}Pb size distributions in ambient aerosol. Atmos. Environ. 32, 983–991. http://dx.doi.org/10.1016/S1352-2310(97)00333-6.
Xie, P., Arkin, P.A., 1997. Global precipitation: a 17-year monthly analysis based on gauge observations, satellite estimates, and numerical model outputs. Bull. Am. Meteor. Soc. 78, 2539–2558.
Young, J.A., Silker, W.B., 1980. Aerosol deposition velocities on the Pacific and Atlantic oceans calculated from ^{7}Be measurements. Earth Planet. Sci. Lett. 50, 92–104.